SEQUENTIAL MEASUREMENTS METHOD FOR MOVING SURFACES PROFILING

by

JAVIER IGNACIO GAZZARRI

Ingeniero Mecánico, Universidad de Buenos Aires, 1998

A THESIS SUBMITTED IN PARTIAL FULFILMENT OF
THE REQUIREMENTS FOR THE DEGREE OF

MASTER OF APPLIED SCIENCE

in

THE FACULTY OF GRADUATE STUDIES

(Department of Mechanical Engineering)

We accept this thesis as conforming
to the required standard

THE UNIVERSITY OF BRITISH COLUMBIA

June 2003

In presenting this thesis in partial fulfilment of the requirements for an advanced degree at the University of British Columbia, I agree that the Library shall make it freely available for reference and study. I further agree that permission for extensive copying of this thesis for scholarly purposes may be granted by the head of my department or by his or her representatives. It is understood that copying or publication of this thesis for financial gain shall not be allowed without my written permission.

Department of MECHANICAL ENGINEERING

The University of British Columbia
Vancouver, Canada

Date JULY 3rd 2003

DE-6 (2/88)

Abstract

Surface profiling is an important need in many industrial and scientific applications. Lumber manufacture quality control is a typical example.

The simplest way to measure surface height profile is to make a series of measurements with a displacement sensor while relatively moving the specimen and sensor in a straight line perpendicular to the measurement direction. The drawback to this method is that deviations from straight-line motion cause errors that are indistinguishable from measured surface shape. In many cases, linear motion of the required accuracy is not practicable in industrial conditions. The state of the art procedure to monitor surface quality is thickness measurement, which is insensitive to rigid motion. However, it cannot separately identify the surfaces each side of the product, very often machined by different tools.

This work describes a novel method for measuring surface height profile in presence of relative motion between the piece and the sensor and on two sides independently. This is very useful for maintenance purposes because it constitutes a fast and direct way to monitor tool performance online.

The procedure involves using multiple sensors operating along a line in the direction of the object motion. The central idea of the proposed method is the observation that surface height features appear in delayed sequence as the specimen moves sideways relative to the sensor array. However, any relative motions, either vertical or rotational, appear simultaneously at all sensors. The proposed equations constitute an inverse problem, and fitting methods of Inverse Theory are used to separate the delayed and simultaneous components of the measurements, from which the surface height profiles can be reconstructed. The proposed equations were applied on an experimental conveyor with several laser sensors on different scanning configurations. Surface calculations adequately met accuracy requirements of lumber inspection standards.

The proposed method is capable of profiling two sides of an object, separately and independently of relative motions between the sensors and the surfaces. If parallel lines are scanned on the same side of the object, information about overall twist is also obtained.

Table of Contents

List of Figures

List of Symbols and Abbreviations

$\boldsymbol{a}, \boldsymbol{b}, \boldsymbol{c}, \boldsymbol{d}, \boldsymbol{e}, \boldsymbol{f}, \boldsymbol{g}, \boldsymbol{h}$	sensors
SE	Sequential Equations
$\boldsymbol{A}$	system matrix
g^{OBS}	observed data vector
f	model vector
Φ	least-squares functional
Φ^{TIKH}	regularized least-squares functional
SVD	singular values decomposition
β	regularization factor
$\alpha_{small}\ \alpha_{flat}\ \alpha_{smooth}$	penalty weights
$W_{small}\ W_{flat}\ W_{smooth}$	0^{th}, 1^{st} and 2^{nd} order discrete derivative operators
p, q, r, s	distances between consecutive sensors
m	mid-span length of sensors array
D	total span of sensors array
x	distance from surface start point to sensor $\boldsymbol{a}$
L	profiled length
$a_i, b_i, c_i, d_i, e_i, f_i, g_i, h_i$	data vectors from each sensor
u	upper surface profile height
v	lower surface profile height
u^F	front upper surface profile height
u^B	back upper surface profile height
v^F	front lower surface profile height
v^B	back lower surface profile height
w	vertical translational rigid body motion
θ	rotational rigid body motion about sensors mid-span (*pitch*)
z	scaled pitch ($= \theta \times m$)
ϕ	rotational rigid body motion about longitudinal axis (*roll*)
Δ	distance between parallel scan lines
y	scaled roll ($= \phi \times \Delta/2$)

i	measurement index
shift	array offset on parallel scan lines
ns	number of sensors
n	number of points along profile
N	total number of data points
M	total number of unknown variables
ndata	number of data points per sensor
λ	wavelength
σ	data standard deviation
ε	data misfit
MCO	mid-chord offset
U	amplitude of generic long wavelength features
κ	curvature
δ	bending deflection at mid-span

Acknowledgements

My most sincere gratitude goes to my supervisor, Dr Gary Schajer for his personal, academic and financial support. I am able to present a work of which I feel proud thanks to his guidance and intellectual generosity.

Nothing of what I did could have been done if it were not for my wife, Veronica, who trusted in our Canadian adventure and helped to make my dream come true.

Truth is what stands the test of experience

Albert Einstein

CHAPTER 1. Introduction

Increasing costs of raw materials and finished products demand a more efficient use of the resources in many industrial activities.

Lumber production is a notable example of such activities because of the unusually high cost of wood. Accordingly, sawmill managers are making great efforts to maximize log throughput in order to remain competitive [1]. Machine centers must saw smoothly and accurately to keep allowances as small as possible.

The extremely high production output rate of a sawmill represents a very demanding requirement for a reliable online inspection system. Moreover, physical and environmental conditions in a sawmill make the implementation of any inspection apparatus difficult in the sense that it will be exposed to vibrations and dust, as well as uncontrolled temperature and humidity conditions.

Given the high production rates involved, it is desirable to have a system scanning all pieces rather than a batch selection. Any cutting tool malfunctioning should be corrected as soon as possible to prevent an excessive number of pieces from being defective. This is a far more stringent procedure than it is product statistical control inspection, in which only a reduced number of pieces can be inspected offline to get satisfactory results.

Surface profiling of sawn lumber pieces is an effective means of assessing cutting tool performance. If sawn pieces can be inspected continuously after a certain production stage in the sawmill, immediate feedback about tool performance is available and prompt maintenance corrections can prevent the given machine from sawing an excessive number of defective boards.

The question that arises is: How can this be achieved in a sawmill? Lumber is transported along imprecise rollers or chain-driven conveyors, and it is necessary to detect patterns of the order of half a millimeter of amplitude. This basic question states the first requirement of an inspection system of this kind: rigid body motions of the scanned piece must be removed from the signal.

Thickness measurement is the state-of-the-art online sawmill procedure to monitor cutting processes because the subtraction of two opposing distance signals (which is the piece thickness) filters out any rigid motion, common to both sides of a solid piece. Thickness information meets general purposes of quality control, but it also suffers from some limitations such as loss of individual information from each surface, very often machined by different tools. If the purpose of the inspection is to have useful information about a cutting tool's performance and this information must be used to take corrective maintenance actions, it is essential for it to give individual information about each cutting tool rather than a combination of both.

Thus, there is a need to have two individual profiles per board, and these profiles must be calculated from data acquired while the specimen is traveling along a conveyor, experiencing rigid motion in the direction of the measurement.

The objective of the present work is to develop a system that is capable of giving individual profiles along one or more lines in the surface of two-sided long objects, removing any rigid motion from of the signal.

This is achieved by scanning the lines sequentially with multiple sensors. The central idea of the proposed method is that surface shape features appear in delayed sequence as the specimen moves sideways relative to a multiple sensor array. However, any relative motions,

either vertical or rotational, appear simultaneously at all sensors. The signal appearing in each sensor is expressed as a combination of surface profile and rigid motion, both of them unknown. This idea can be extended to the measurement of several parallel profiles, on the same or opposite surface of the specimen. The same rigid motions appear at all sensors. This feature provides increased opportunity for averaging and a more efficient use of measured data.

The need to separate surface shape from rigid motion out of data containing a combination of them gives the problem the characteristics of an inverse problem. This kind of problems appears in a variety of disciplines, mainly where there is a model to be reconstructed out of indirect measurements. A distinctive characteristic of inverse problems is their ill-posedness [2]. It implies that under certain conditions the problem becomes unstable and the solution may change dramatically due to small changes in the data, namely addition of noise. Under certain circumstances, their solution can also be non-unique. All these features had to be taken into account to find solutions to the proposed equations, making use of mathematical tools derived from Inverse Theory.

The present work is organized as follows. Chapter 2 gives an outline of existing methods for profiling in the presence of relative rigid motion between the sensor and the surface to be measured. It also points out their limitations and reasons for which they are not suitable for the purposes of this project.

Chapter 3 introduces the mathematical background of the proposed method. In a sequence of progressively increasing complexity, this chapter describes the fundamental equations and their main characteristics, as well as problems arising from their ill-posedness. It also gives a description of how methods of Linear Inverse Theory are used to find suitable solutions to

the equations. Finally, regularization techniques are introduced as a means to mitigate the noise amplification in large systems and to provide a solution when the configuration is rank deficient.

Chapter 4 details the experimental part of the research work. A brief description of the sensors and a laboratory conveyor is followed by several surface reconstructions obtained from real data. The examples illustrate the cases explained in the previous chapter. It follows the description of a second conveyor, more closely representative of industrial set-ups, which was used to scan real lumber pieces. Typical patterns of defective sawing are presented as examples of the capabilities of the system. The chapter concludes with a discussion about artifacts observed in situations where the inherent assumptions of the method are not met and a brief description of a possibly interesting alternative for the solution of the proposed equations.

Chapter 5 gives conclusions and an overall assessment of the capabilities and limitations of the system and recommendations for future work.

CHAPTER 2. Background and Literature Review

Surface profiling in presence of relative motion between the sensors and the surface is a very important inspection technique in activities such as wood sawing, railway maintenance [3, 4, 5] and highway leveling [6, 7]. For the first case, the relevance stems from the fact that it is not possible to make the wood board move along a straight line on a sawmill conveyor. For the last two cases, it is obviously not possible to profile railways or highways from a flat reference frame, but from an apparatus traveling along them. In all the aforementioned examples, it is necessary to measure the profiles in the presence of relative rigid motion between the sensors and the surface.

For the lumber industry in particular, given that raw wood can account for up to 75% of the total cost of a wood product such as lumber [8], surface profiling is an important method for assessing cutting tool performance, thereby reducing wood wastage. Current sawmill product monitoring is done by *thickness measurement*, either by hand (using calipers) or measuring distances to both surfaces from two opposing sensors and then subtracting the signals [9]. In this second case, any rigid body motion component contained in the data, common to both sides of the specimen, is cancelled out and the result obtained is the thickness of the product along its length.

Even when this magnitude gives an idea of the overall appearance of the product, it suffers from a serious drawback: individual information from each side is lost in the subtraction. Therefore, it is not possible to know the individual shapes of the two surfaces by using the thickness value. Obtaining individual profiles from each side is, however, a desired outcome from the sensor system, because very often two different blades cut each side of the board. If

the purpose is to evaluate the cutting tools condition, it is necessary to determine how each individual blade is performing. This information would provide a useful and more complete insight to the sawmill operators regarding cutting conditions, making possible to take quick maintenance decisions to prevent excessive production of defective pieces.

Another widely used profiling method that is insensitive to relative motions between scanned piece and sensor is *curvature integration*, because a discrete approximation to surface curvature can be identified independently of rigid translations or rotations. This method is especially useful in fields such as railway and highway maintenance, where the sensors must be attached to a vehicle traveling along the surface to be scanned, and consequently experiencing relative rigid motion because of surface and vehicle wheel irregularities. This technique has been used for half a century, and Cooper describes the traditional sensors configuration in [5].

The curvature can be estimated from the second finite difference of the three-points measurement using the "mid-chord offset" (*MCO*):

$$MCO = \frac{a - 2b + c}{2}$$

where a, b and c are the three equally-spaced sensors readings.

The MCO is related to the finite differences approximation to the curvature κ:

$$\kappa(i) \cong \frac{2f_i - f_{i-1} - f_{i+1}}{h^2} = -\frac{2\,MCO}{h^2}$$

where h is the discretization step.

The curvature obtained from the MCO is integrated twice to determine the surface profile.

The curvature integration method is subject to practical limitations that appear at both ends of the spatial frequency response range.

Measurement noise blurs the small differences in sensor measurements that occur when measuring surface profiles with long wavelengths. The maximum observable wavelength is $\lambda_{max} \approx \frac{\pi}{2} h \sqrt{\frac{U}{\sigma}}$, where h is the spacing between the outer two sensors (the "chord length"), U is the surface profile amplitude, and σ is the standard deviation of the measurement noise.

Spatial discretization error limits the shortest wavelength that can be accurately identified in a surface profile to $\lambda_{\min} \approx h$. In addition, wavelengths that are integer fractions of the sensor spacing, "nulls", are completely attenuated.

The high-frequency response can be improved by moving the sensors closer together, while the low-frequency response is improved by moving them further apart. Using an asymmetrical sensor arrangement can reduce the occurrence of nulls as showed by Takeshita [10], but they cannot be totally eliminated.

In general, curvature integration methods are only reliable for certain wavelengths and sinusoid-shaped surfaces and do not give reliable results when applied to sharp features, acting as a filter. Buhler [11] describes a contact multi-sensor apparatus with several curvature-measurement arrays, one for each different range of wavelengths, in an attempt to extend the system capability to wider spectra.

A further weakness of curvature methods is that they typically use only part of the information content available from the measured data. They use the instantaneous part of the data, the local curvature estimate, but they do not use the geometrical relationships that exist among successive measurements. This is a clear disadvantage in what concerns random

noise compensation, because no data averaging takes place.

Corbin [12] describes an interesting four-sensor method that seeks to address the wavelength and null limitations, as well as to include the geometric relationships between successive measurements, but his description leads to a non-unique solution. However, his ideas played a very important role in the development of the method proposed in this work, for he appears to be the first to describe a way to overcome the trade-off between short and long wavelength resolution in curvature integration techniques with only one set of sensors. In his patent, he describes a four sensors array to measure distances to the profiling surface at each sampling interval. The measurements have to be combined to transform an asymmetric chord offset, calculated using the distances between sensors, into a mid-chord offset that would result of taking samples with three virtual sensors hypothetically separated one step interval apart.

An alternative approach, the *inertial method*, uses an accelerometer that runs at a constant speed along the surface to be profiled, giving a signal that is proportional to surface curvature [4]. As before, the signal is integrated twice to obtain the surface shape. Conceptual simplicity makes this an attractive method. However, there are also some practical limitations. The first concerns the high frequencies that need to be measured in the lumber industry, related to the wavelengths of the sawing patterns and the lumber board speed. These can extend beyond the capabilities of the accelerometer. A second limitation is the assumption that the accelerometer and the surface are permanently in contact. This is difficult to achieve reliably, especially at high scanning speeds due to the large inertial forces that act on the system. Finally, only smooth profiles can be measured. A sharp step, for example, would not be detected properly, apart from being a potential danger for the mechanical integrity of the apparatus.

Modern railway and road profilers combine displacement sensors and accelerometers to seek to combine the particular advantages of the two measurement principles [13]. The accelerometer signal gives an inertial reference frame for a range optical sensor. The fact that the accelerometer has to be mechanically connected to the profiled surface makes this choice unsuitable for lumber profiling.

CHAPTER 3. Sequential Equations

3.1 Introduction

The idea behind the proposed method is to scan the profiling surface sequentially to identify a repetitive delayed pattern from a non-repeated simultaneous pattern in the acquired signal. The former corresponds to the surface profile and the latter corresponds to the rigid body motion of the specimen. This is achieved by taking multiple measurements of every point to be profiled along one or more lines on the sample surface. The Sequential Equations (SE) give the relationship between the sequentially acquired data and the combination of surface profile and rigid body motion.

The simplest case of two sensors measuring distance to a given surface is useful to describe the main idea underlying the proposed method. A description of more complex cases will be given in subsequent sections.

3.2 Two sensors – no rotation

Let two fixed sensors ***a*** and ***b*** act upon one of the surfaces of a long object moving from left to right. The line defined by them is aligned with the direction of relative movement of the surface. The description is also valid for the case in which the sensors move and the surface is stationary, or even for both moving relative to a fixed frame of reference. For initial simplicity, let us also restrict the rigid motion to a vertical and purely translational displacement. Conceptually, this could occur in a roller conveyor system, such as that shown in Figure 1, which has eccentrically pinned circular rollers. If the rollers are equal and rotate

in-phase, the specimen translates vertically while moving horizontally from left to right.

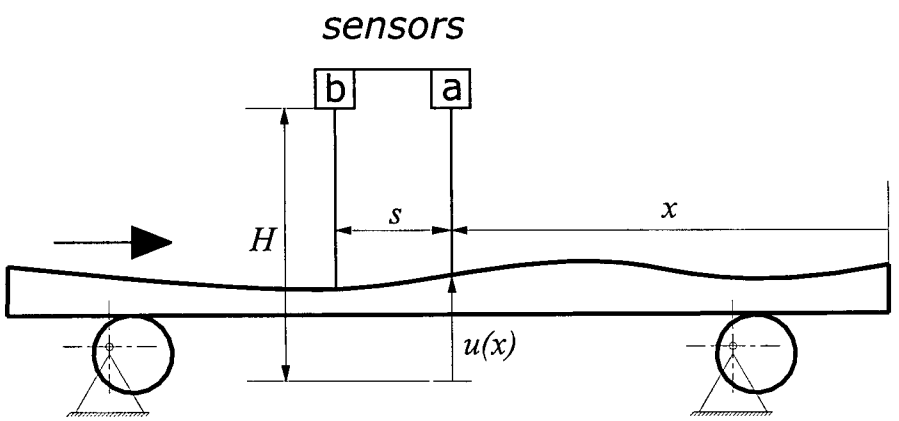

Figure 1 Two sensors arrangement for purely translational vertical motion

The geometry in Figure 1 creates an inversion of the measured surface data. An increase in surface height causes a decrease in sensor reading. To avoid possible confusion, it is convenient to define a "height" quantity of the kind:

$$a(x) = H - a^*(x) \tag{1}$$

where $a(x)$ is the inverted distance, $a^*(x)$ is the measured distance of the surface from sensor ***a***, H is a distance from sensor ***a*** to an arbitrary reference line, and x is the distance from the start of the specimen to sensor ***a***. The exact value chosen for H is not critical for one-sided measurements.

For the arrangement shown in Figure 1, the sensor measurements are, at a given instant:

$$\begin{aligned} a(x) &= u(x) + w(x) \\ b(x) &= u(x+s) + w(x) \end{aligned} \tag{2}$$

where

x = distance from the start of the specimen to sensor ***a***

$a(x)$, $b(x)$ = "height" data acquired by the sensors, positive upwards

$u(x)$ = surface topography, measured from a reference line, positive upwards

$w(x)$ = rigid body vertical translation, positive upwards

s = distance between the two sensors

The terms $a(x)$ and $b(x)$ refer to the "height" data acquired by the sensors when the specimen has moved a distance x beyond sensor ***a***. The variable x in equation (2) has a dual character. When associated with the surface profile $u(x)$, it is a spatial coordinate describing the distance along the surface. However, for all other quantities, it is a quasi-temporal quantity. It refers to the values of those quantities that exist at the same time as sensor ***a*** measures surface point $u(x)$. This dual definition is used to emphasize that the distance s in equation (2) is the fundamental quantity for describing the delay seen when observing surface features by successive sensors, not the particular time taken to move that distance. This choice of variable eliminates any requirement that the conveyor system in Figure 1 should move at a uniform speed. However, for uniqueness, there should be no periods of zero speed.

The terms $w(x)$ in equation (2) refer to the coincident vertical displacement of a horizontal reference line fixed on or adjacent to the specimen. Note that this rigid-body displacement refers to the entire reference line, and is therefore the same at all displacement sensors. The terms $u(x)$ and $u(x+s)$ refer to the surface heights from the reference line, at distances x and $x+s$ from the leading end of the specimen, where s is the distance between sensors. The simultaneous character of the observed rigid-body motions can be seen in equation (2) by the same x coordinate appearing in the terms $a(x)$, $b(x)$ and $w(x)$. The delayed character of the observed surface profile appears in the terms $u(x)$ and $u(x+s)$.

3.3 The problem as an inverse problem

The structure of equations (2) gives the problem the characteristics of an *inverse problem* because a combination of the unknown functions gives the acquired data. The associated *forward problem* is: given a surface profile $u(x)$ and a vertical rigid motion $w(x)$, find the signal that would be acquired by each sensor. Inverse problems have been extensively studied and the techniques developed to cope with their difficulties constitute a discipline called *Inverse Theory*. Inverse problems are known to be ill-posed and their solution may be non-unique. Ill-posedness implies that very small changes in the data may result in very large changes in the solution, leading to unstable systems. These problems will be addressed in detail later in this and the next chapter (section 3.10).

3.4 Discretization

Typically measurements $a(x)$ and $b(x)$ are made at a series of n equally spaced points along the specimen. In this case, the continuous functions $a(x)$, $b(x)$, $u(x)$ and $w(x)$ transform into discrete functions a_i, b_i, u_i and w_i, where i is a positive index. The number of measurement steps is such that the scanning begins when the first surface point is seen by sensor $\boldsymbol{a}$ and ends when the last surface point is seen by sensor $\boldsymbol{b}$. This procedure is consistent along the entirety of this work. The number of data points per sensor is therefore $n - p$, where p is the number of measurement intervals between sensors $\boldsymbol{a}$ and $\boldsymbol{b}$, corresponding to distance s. Equations (2) then become:

$$\begin{aligned} a_i &= u_i + w_i \\ b_i &= u_{i+p} + w_i \end{aligned} \qquad \text{for } 1 \le i \le n-p \tag{3}$$

where:

i = measurement index, $1 \le i \le n-p$

a_i, b_i = measured surface heights relative to an arbitrarily chosen horizontal reference line

u_i = surface height profile, positive upwards

w_i = rigid-body vertical translation at instant i, positive upwards

The relationships between the quantities in equations (3) are purely geometrical, and can be expressed in matrix form. For example, when $n = 6$ and $p = 2$:

$$\left[\begin{array}{cccc:cccc} 1 & & & & 1 & & & \\ & 1 & & & & 1 & & \\ & & 1 & & & & 1 & \\ & & & 1 & & & & 1 \\ \hdashline & 1 & & & & 1 & & \\ & & 1 & & & & 1 & \\ & & & 1 & & & & 1 \end{array}\right] \left[\begin{array}{c} u_1 \\ u_2 \\ u_3 \\ u_4 \\ u_5 \\ u_6 \\ \hdashline w_1 \\ w_2 \\ w_3 \\ w_4 \end{array}\right] = \left[\begin{array}{c} a_1 \\ a_2 \\ a_3 \\ a_4 \\ \hdashline b_1 \\ b_2 \\ b_3 \\ b_4 \end{array}\right] \tag{4}$$

corresponding to:

$$A\, f = g^{obs} \tag{5}$$

where $\boldsymbol{f}$ and $\boldsymbol{g}^{obs}$ are the *model* and *observed data* vectors respectively.

In general, the *non-dimensional* system matrix $\boldsymbol{A}$, also called the *kernel*, is rectangular, depending on the relationship between the number of sensors and variables. The $2n - p$ columns of this matrix define the system's *model space*, while the $2(n - p)$ rows define its *data space*. Equations (3) do not have a unique solution because the dimension of the model space exceeds that of the data space, i.e., there are p more unknowns than data. Thus, the

model space includes at least p null vectors. These are vectors $\boldsymbol{f_0}$ that when premultiplied by matrix A correspond to a zero data vector $\boldsymbol{g}$. For $n = 6$, $p = 2$, the null model vectors are:

$$\boldsymbol{f_{01}} = [\,1 \;\; 0 \;\; 1 \;\; 0 \;\; 1 \;\; 0 \;\; -1 \;\; 0 \;\; -1 \;\; 0\,]^T \tag{6}$$

$$\boldsymbol{f_{02}} = [\,0 \;\; 1 \;\; 0 \;\; 1 \;\; 0 \;\; 1 \;\; 0 \;\; -1 \;\; 0 \;\; -1\,]^T \tag{7}$$

In equation (4), one "unknown", the initial rigid-body translation, w_1, can be eliminated by arbitrarily assigning it a zero value. This assignment, which eliminates the first null vector, $\boldsymbol{f_{01}}$, involves no loss of generality. However, there remain $p - 1$ null vectors of the type shown in equation (7). Consequently, for $p > 1$, there is no unique solution.

Physically, the null vectors correspond to particular surface shapes and rigid motions that cannot be distinguished by the sensor configuration. For example, consider the arrangement shown in Figure 2, comprising two sensors scanning a surface, p sampling intervals apart.

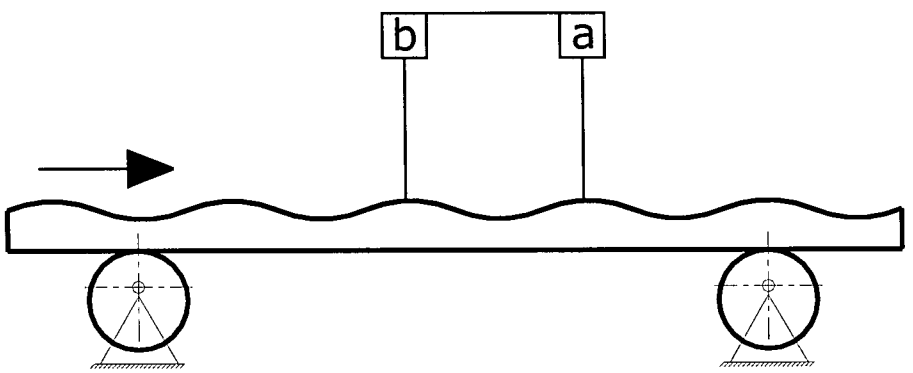

Figure 2 Physical interpretation of a null vector
Vertical motion is in counterphase with the profile, such that the sensors detect no change

In this particular example, the specimen surface happens to be sinusoidal with period equal to

p sampling intervals. The rollers also happen to be mounted eccentrically. Their circumference, eccentricity and phase are such that the resulting rigid-body translation is sinusoidal with the same amplitude and wavelength as the surface shape, but with opposite phase. Under these conditions, the surface shape and the rigid-body translation of the sample counteract each other. The two effects sum to zero, and the sensors detect nothing. This zero detection corresponds to a null model vector.

3.5 Three sensors – no rotation

The mathematical difficulties encountered when attempting surface profiling with two sensors stem from insufficiency of data. This issue can be relieved by the addition of a third sensor, as shown in Figure 3.

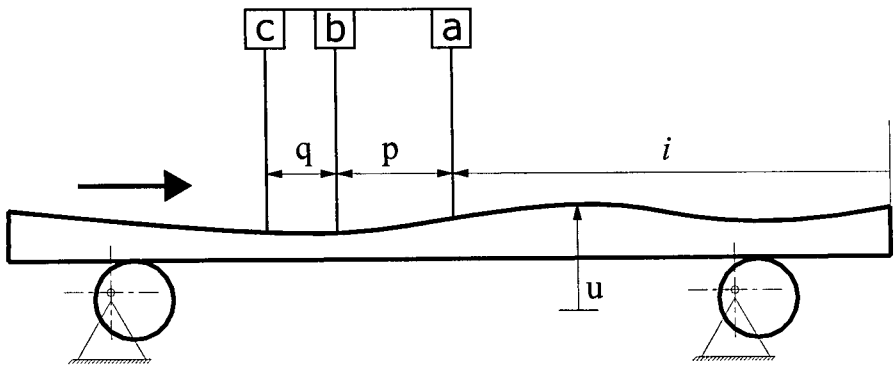

Figure 3 Three sensors arrangement

For this case, equations (3) expand to:

$$\begin{aligned} a_i &= u_i + w_i \\ b_i &= u_{i+p} + w_i \\ c_i &= u_{i+p+q} + w_i \end{aligned} \qquad \text{for } 1 \le i \le n-p-q \tag{8}$$

Where p and q are the number of measurement intervals between sensors $\boldsymbol{a}$ and $\boldsymbol{b}$, and between $\boldsymbol{b}$ and $\boldsymbol{c}$, respectively. For $n = 7$, $p = 2$, and $q = 1$, the system equation becomes:

$$\left[\begin{array}{ccccc|ccccc} 1 & & & & & 1 & & & & \\ & 1 & & & & & 1 & & & \\ & & 1 & & & & & 1 & & \\ & & & 1 & & & & & 1 & \\ \hline & 1 & & & & 1 & & & & \\ & & 1 & & & & 1 & & & \\ & & & 1 & & & & 1 & & \\ & & & & 1 & & & & 1 & \\ \hline & & & 1 & & 1 & & & & \\ & & & & 1 & & 1 & & & \\ & & & & & 1 & & 1 & & \\ & & & & & & 1 & & 1 & \end{array}\right] \left[\begin{array}{c} u_1 \\ u_2 \\ u_3 \\ u_4 \\ u_5 \\ u_6 \\ u_7 \\ \hline w_1 \\ w_2 \\ w_3 \\ w_4 \end{array}\right] = \left[\begin{array}{c} a_1 \\ a_2 \\ a_3 \\ a_4 \\ \hline b_1 \\ b_2 \\ b_3 \\ b_4 \\ \hline c_1 \\ c_2 \\ c_3 \\ c_4 \end{array}\right] \tag{9}$$

There are now $3\ (n - p - q)$ data and $2n - p - q$ unknowns. A necessary, although not sufficient condition for a solution to exist is that the number of data should equal or exceed the number of unknowns. In equation (9), this implies $n \geq 2\ (p + q)$. As before, equation (9) has been written to cover the period over which all the sensors are able to make measurements, that is to say $n - p - q$ data points per sensor. This is convenient for practical applications because the same number of measurements are made by all sensors, minimizing the number of rigid motion unknowns.

Even when there are as many or more data than unknowns, equation (9) cannot directly provide the desired solution. This is because the system matrix in equation (9) is not full-rank in columns. There exists a null model vector similar to $\boldsymbol{f_{01}}$ in equation (6). As before, this null can be eliminated without loss of generality by arbitrarily assigning a zero value to the initial rigid-body translation w_1.

Other null model vectors similar to $\boldsymbol{f_{02}}$ in equation (7) can also exist. The simplest example

would occur with equi-spaced sensors, i.e., when $p = q$. The associated null model vector corresponds to the physical arrangement in Figure 2, where a third sensor is added with a separation of one or more wavelengths. As before, such a system would be unable to distinguish a sinusoidal surface profile from a sinusoidal rigid-body translation. Even for unequally spaced sensors, null model vectors also exist when p and q share a common factor other than one. In this case, the behaviour illustrated in Figure 2 occurs for a shorter surface wavelength equal to the common factor times the measurement spacing.

After setting $w_1 = 0$ and ensuring that $n \geq 2\,(p + q) - 1$ and that p and q have no common factors, it is possible to proceed with the solution of equation (9). Typically, matrix $\boldsymbol{A}$ is rectangular ($N \times M$) with $N > M$ (excess data) to provide the system with data averaging, and the solution cannot be found via the matrix inverse but minimizing some *measure* of the difference:

$$A f - g^{obs} \tag{10}$$

The most commonly used measure is the 2-norm (Euclidean Norm) defined as the square root of the inner product of a vector with itself:

$$\| \cdot \| = [(\cdot, \cdot)]^{1/2} \tag{11}$$

For this case, a *misfit functional* is defined as:

$$\Phi(f) = \| A f - g^{obs} \|^2 \tag{12}$$

The Least Squares approximation f_{LS} is the solution of

$$\min_f \left(\| A f - g^{obs} \|^2 \right) \tag{13}$$

The solution is found by differentiating the misfit functional with respect to $\boldsymbol{f}$ and equating

the result to zero. For over-determined systems, this is equivalent to pre-multiplying equation (5) by the transpose of the system matrix A to obtain a system known as the "Normal Equations" [2]:

$$A^T A\ f\ =\ A^T g^{obs} \tag{14}$$

For the example case in equation (9), the Normal Equations (after setting $w_1 = 0$) are:

$$\left[\begin{array}{ccccccc|ccc} 1 & & & & & & & 1 & & \\ & 1 & & & & & & & 1 & \\ & & 2 & & & & & & 1 & \\ & & & 3 & & & & 1 & & 1 \\ & & & & 2 & & & 1 & 1 & \\ & & & & & 2 & & & 1 & 1 \\ & & & & & & 1 & & & 1 \\ \hline 1 & & 1 & 1 & & & & 3 & & \\ & 1 & & 1 & 1 & & & & 3 & \\ & & 1 & & 1 & 1 & & & & 3 \end{array}\right] \left[\begin{array}{c} u_1 \\ u_2 \\ u_3 \\ u_4 \\ u_5 \\ u_6 \\ u_7 \\ w_2 \\ w_3 \\ w_4 \end{array}\right] = \left[\begin{array}{c} a_1 \\ a_2 \\ a_3 + b_1 \\ a_4 + b_2 + c_1 \\ b_3 + c_2 \\ b_4 + c_3 \\ c_4 \\ a_2 + b_2 + c_2 \\ a_3 + b_3 + c_3 \\ a_4 + b_4 + c_4 \end{array}\right] \tag{15}$$

For small values of n, a general matrix equation solver is sufficient to solve the Normal Equations. Matrix $A^T A$ is symmetrical and its elements can be reordered so as to have a banded structure, so some computational economy can be achieved by using a specialized solver for symmetric banded matrices [14], especially for larger values of n.

As an illustration of the proposed method, consider the following numerical example. A hypothetical specimen, *1m* long, is profiled at *10mm* intervals using $n = 101$ sampling points. A three-sensor arrangement is used, with spacings between the sensors of *50mm* and *80mm*. This corresponds to $p = 5$ and $q = 8$. The specimen surface is flat, except for two square steps *1mm* high and *50mm* wide. It undergoes a sinusoidal rigid-body motion of amplitude *1mm* and wavelength *500mm* during the measurement process. Synthetic data were created for this case, with added pseudo-random noise, normally distributed with a standard

deviation of *0.05mm* and zero mean. Figure 4 shows the generated data and the reconstructed surface. Both the high-frequency part of the surface profile, the steps, and the low-frequency part, the flat background, are successfully reconstructed.

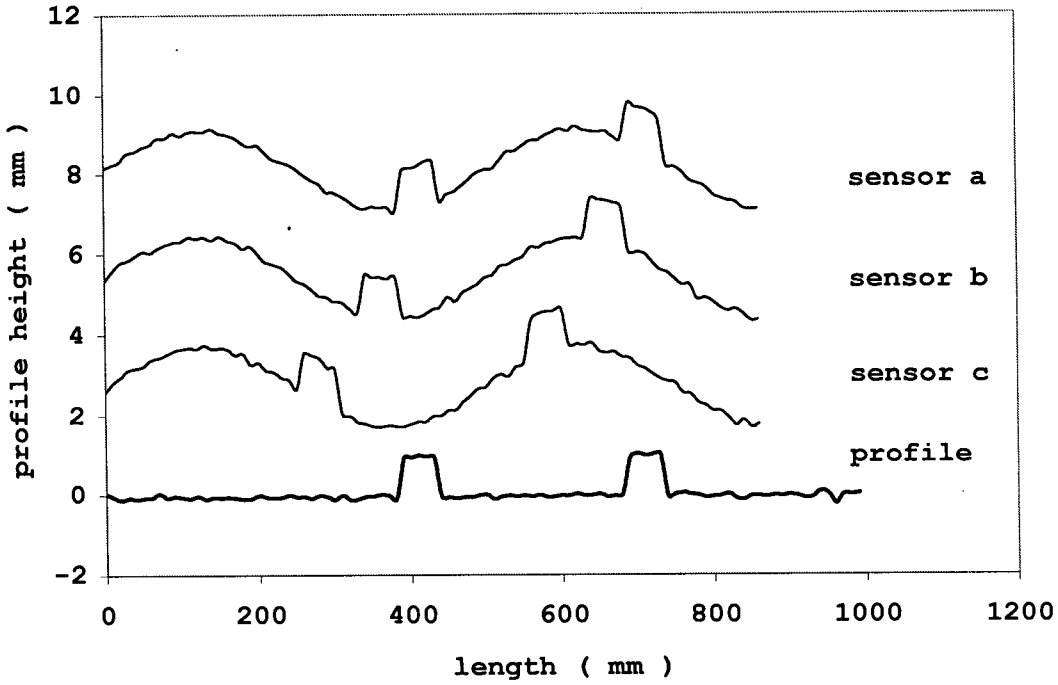

Figure 4 Three sensors reconstruction
Flat surface with two square bumps and sinusoidal vertical translation

3.6 Rigid body rotation

In most practical situations the rigid body motion will always have a rotational component in the plane defined by the scanned line and the sensors beams. This type of movement is known as *pitch*. Inclusion of rigid-body rotation adds an extra degree of freedom to the mathematical model, and correspondingly increases the amount of data required for a solution. At least four sensors are required to achieve a full-rank solution for one-sided profiling including rotation. Please see Appendix I for a general expression of the minimum

required number of sensors.

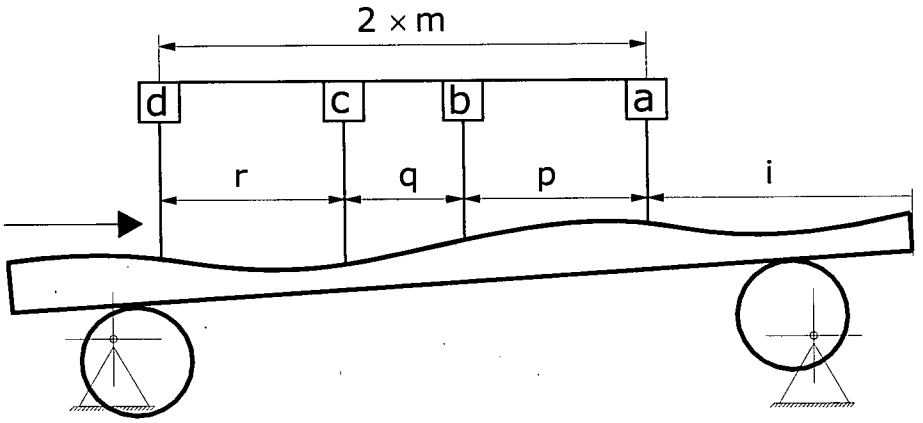

Figure 5 One-sided profiling with rotation
One extra sensor is necessary

Figure 5 shows a typical sensor arrangement. The arrangement of eccentrically mounted rollers schematically indicates that the specimen motion can include both translation and rotation. For measurements made at n equally spaced points along the specimen, the sensor measurements combine the surface profile and rigid-body motions as follows:

$$\begin{aligned} a_i &= u_i + w_i - z_i(-m)/m \\ b_i &= u_{i+p} + w_i - z_i(p-m)/m \\ c_i &= u_{i+p+q} + w_i - z_i(p+q-m)/m \\ d_i &= u_{i+p+q+r} + w_i - z_i(p+q+r-m)/m \end{aligned} \qquad 1 \le i \le n-p-q-r \tag{16}$$

where:

a_i, b_i, c_i, d_i = measured surface heights relative to an arbitrarily chosen horizontal reference line

u_i = surface height profile, positive upwards

w_i = rigid-body vertical translation at instant i, positive upwards

z_i = scaled rigid-body rotation centred midspan of sensor array at instant i, positive counter-clockwise

p, q, r = number of measurement intervals between successive sensors

m = half span length of the sensor array $= (p + q + r) / 2$

To provide a unique solution, the initial rigid body translation and rotation w_1 and z_1 are each chosen as the zero data for these quantities. This does not involve any loss in generality. For dimensional consistency and numerical stability, the rotation variable is scaled as $z_i = \theta_i \times m$, where θ_i is the angular rotation (in radians) and m is half the total span of the sensor array so that variables u, w and z have similar size. It is assumed that the rotation angle is sufficiently small that $\theta \approx tan\theta$. In equation (16), the center of the rigid-body rotation is defined to be at the midpoint of the sensor array. Again, this does not involve any loss in generality. The midpoint was selected because it gives a convenient symmetry in the normal equations matrix.

The relationships among successive measurements of the quantities in equations can be expressed in matrix form as before.

Although, in principle, any choice of distances between sensors can be utilized provided the non-common-factor requirement is obeyed, long wavelength features are best resolved when the inner two sensors are close to the mid-span, at similar distances to the outer two sensors.

As a general rule, distances between sensors are arranged to detect low frequency features, whereas sample rate is chosen to resolve high frequency shapes and fine details.

3.7 Two-sided profiling

Manufacture of two-sided long flat products often involves machining each face with a different tool. In the lumber industry, for example, several saws cut a big piece of wood to produce many thinner boards.

Thickness measurement is a widely used technique that partially fulfills the need for continuous lumber inspection, but it is unable to provide separate information on each side. It is not possible to individualize a particular saw from the thickness signal only.

One of the most important goals of the present work is to provide a method to profile double-sided flat objects independently on each other in presence of rigid motion. The SE inversion proved to be a plausible approach with promising results.

Two-sided profiling via the SE can be done using a sensor arrangement such as that shown in Figure 6. The attractiveness of this arrangement is that the upper and lower sensors observe the same rigid-body motions. This commonality between both sets of sensors means that only one new variable is introduced, namely the lower surface profile. Thus, a minimum of one additional lower sensor is required to provide the needed additional data, far fewer than the eight needed for two independent profile measurements.

In the arrangement shown in Figure 6, one sensor has been transferred from the upper surface, and two further sensors have been added. Although the sixth sensor is not essential, it is included here to provide a symmetrical arrangement with similar expected measurement accuracy for both sides of the specimen. The additional sensor provides redundant data that is averaged with all the other data. This feature enhances the measurement accuracy for both

sides.

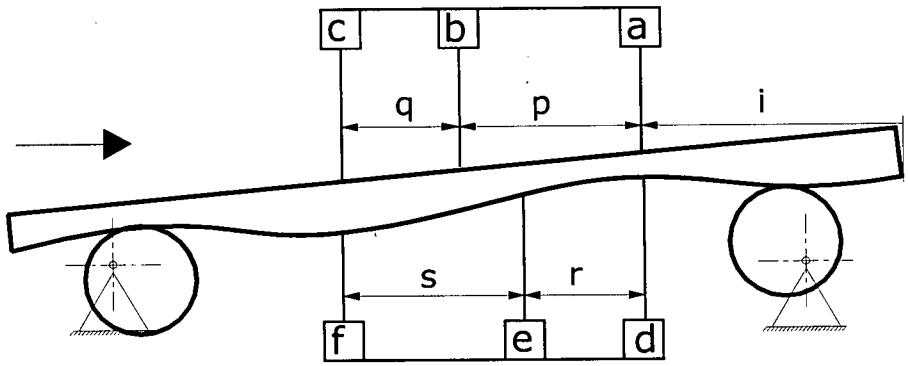

Figure 6 Two-sided profiling with six sensors

For the arrangement in Figure 6, the relationships of the sensor readings to the surface profiles and rigid-body motions are:

$$
\begin{aligned}
a_i &= u_i + w_i - z_i(-m)/m \\
b_i &= u_{i+p} + w_i - z_i(p-m)/m \\
c_i &= u_{i+p+q} + w_i - z_i(p+q-m)/m \\
d_i &= v_i - w_i + z_i(-m)/m \\
e_i &= v_{i+r} - w_i + z_i(r-m)/m \\
f_i &= v_{i+r+s} - w_i + z_i(r+s-m)/m
\end{aligned}
\qquad 1 \le i \le n-p-q \qquad (17)
$$

with $m = \frac{p+q}{2} = \frac{r+s}{2}$

The equations only involve a new surface profile variable, v_i, but no additional rigid-body motions. As previously observed, to achieve a full-rank matrix, the sensor spacings should not have any common factors other than unity. The skew-symmetric arrangement in Figure 6 is chosen to avoid nulls and any left-to-right bias or difference in detection accuracy. The two middle sensors, ***b*** and ***e***, must not be collinear, even when p and q have no common

factors, as a minimum of four independent places must be measured along the longitudinal axis when rotation is included in the calculation. These two sensors, however, should not be taken too far apart from the vertical symmetry line, because long wavelength features are best detected with the middle sensors close to the midpoint between the two outermost sensors.

An important geometrical feature of the arrangement in Figure 6 is the opposing alignment of at least one pair of sensors, for example sensors ***a*** and ***d***. The corresponding lines in equations (17) add together to give specimen thickness without involving the rigid motions w_i and z_i. In this case, the two-sided profiling performed by the sensor arrangement in Figure 6 preserves specimen thickness relationships, even in the presence of possible errors in identifying rigid-body motions. Thus, the advantages of conventional thickness measuring techniques are not lost. This behaviour contrasts with curvature-based methods, where thickness information is lost because the two sides are evaluated independently.

3.8 Parallel profiling

The exploitation of common components in the measurements from multiple sensors can be carried a further step. Practical specimens are often quite wide in the direction out of the paper in Figure 6. In such cases, it can be of interest to measure the surface profile along parallel lines on one or both sides. This generalization introduces an additional rigid-body motion involving rotation around the longitudinal axis of the specimen. The surface profile feature corresponding to this new degree-of-freedom is specimen *twist*, a geometrical characteristic of practical interest.

Parallel profile measurements are possible for both single- and double-surface profiling.

Figure 7 shows an arrangement of six sensors for doing one-sided profiling along two parallel paths. As before, a skew-symmetrical arrangement is chosen to obtain four measurement places along the scanned line and give equal expected calculation accuracy along each surface profile, with the two middle sensors close to the symmetry plane to improve long wavelength resolution capability. In this case, the number of sensors used equals the minimum required to achieve an over-determined system, and the system is not as redundant as in the two-sided case because of the addition of a new degree of freedom, namely the board *roll*.

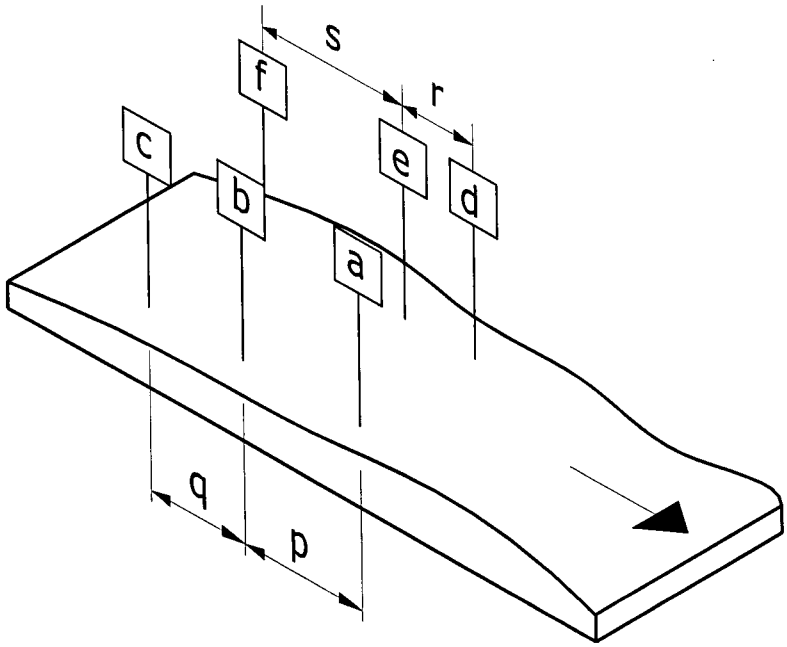

Figure 7 One-sided parallel profiling

For the sensor arrangement shown in Figure 7, the relationships of the sensor readings to the surface profiles and rigid-body motions are:

$$
\begin{aligned}
a_i &= u^F{}_i + w_i + y_i - z_i(-m)/m \\
b_i &= u^F{}_{i+p} + w_i + y_i - z_i(p-m)/m \\
c_i &= u^F{}_{i+p+q} + w_i + y_i - z_i(p+q-m)/m \\
d_i &= u^B{}_i + w_i - y_i - z_i(-m)/m \qquad 1 \le i \le n-p-q \\
e_i &= u^B{}_{i+r} + w_i - y_i - z_i(r-m)/m \\
f_i &= u^B{}_{i+r+s} + w_i - y_i - z_i(r+s-m)/m
\end{aligned}
\tag{18}
$$

Where $u^F{}_i$ and $u^B{}_i$ are the front and back parallel surface profiles respectively, and

$$y_i = \phi \frac{\Delta}{2}$$

corresponds to the rigid-body rotation around the longitudinal axis of the specimen by an angle ϕ, with a distance Δ between the parallel paths.

The assumption of small rotations ($\phi \approx 0$) is also present in this formulation and is consistent with the assumption that even when the specimen rolls, each array measures along a line. For example, if $\phi = 10^\circ$ and $\Delta = 140mm$, the lateral discrepancy is of the order of $1mm$, which in the case of this work can be tolerated.

Specimen twist is given by the expression

$$TWIST_i = \left(u_i^F - u_i^B\right) \tag{19}$$

Unfortunately, twist is not automatically included in equations (18) as in the case of thickness, so the accuracy in its calculation is limited to the capability of the system to resolve long wavelength features.

3.9 Two-sided parallel profiling

The last case of study that combines features of all the aforementioned configurations consists in measuring on both sides of a specimen along two lines per side. This arrangement synthesizes the capabilities of the method and its equations can easily be generalized to any number of profile lines and sensors on both sides. The number of unknown variables is now seven, namely u^F, u^B, v^F, v^B, w, y and z. The required number of sensors to obtain an over-determined system is eight. The preferred configuration is that schematically shown in Figure 8.

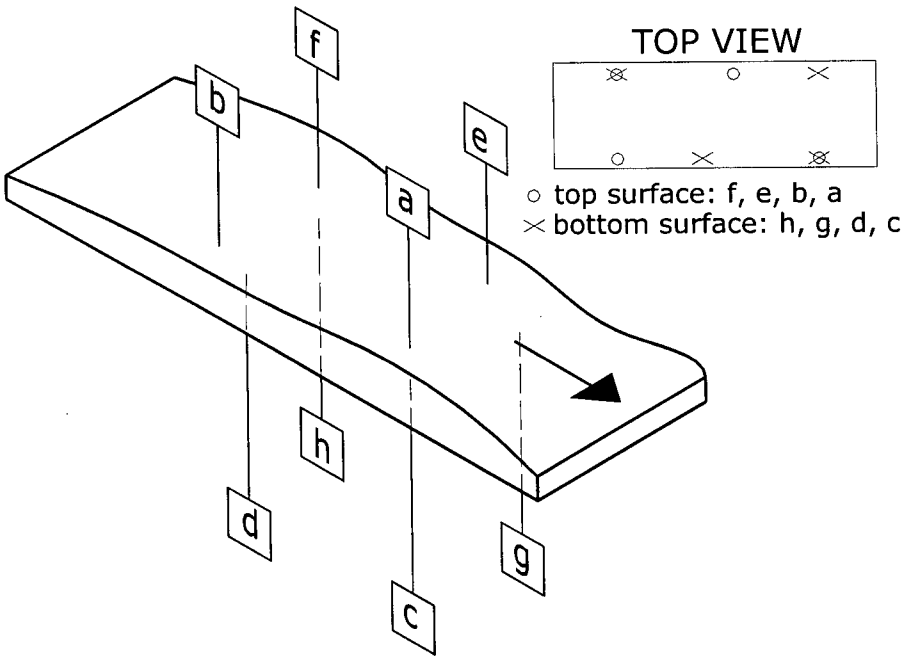

Figure 8 Two-sided parallel profiling

The system of equations to be solved is:

$$
\begin{aligned}
a_i &= u^F{}_i + w_i + y_i - z_i(-m)/m \\
b_i &= u^F{}_{i+p} + w_i + y_i - z_i(p-m)/m \\
c_i &= v^F{}_i - w_i - y_i + z_i(-m)/m \\
d_i &= v^F{}_{i+q} - w_i - y_i + z_i(q-m)/m \\
e_i &= u^B{}_i + w_i - y_i - z_i(shift-m)/m \qquad 1 \le i \le n-p \\
f_i &= u^B{}_{i+r} + w_i - y_i - z_i(shift+r-m)/m \\
g_i &= v^B{}_i - w_i + y_i + z_i(-m)/m \\
h_i &= v^B{}_{i+s} - w_i + y_i + z_i(s-m)/m
\end{aligned}
\tag{20}
$$

Where p, q, r, s are the distances between sensors ***a*** and ***b***, ***c*** and ***d***, ***e*** and ***f*** and ***g*** and ***h*** respectively. The staggered arrangement of sensors creates surface profile reconstructions that differ slightly in length and start points. Set ***e*** – ***f*** is shifted an amount *shift* relative to the vertical plane defined by ***a*** – ***c*** – ***g***. This is a consequence of having only two sensors per scan line, which makes it mandatory to shift the measurement positions in order to avoid singularities.

3.10 Regularization

Rank deficiency and ill-posedness are typical characteristics of inverse problems and they have to be taken into account when noisy data are to be inverted, otherwise the obtained solution will be excessively contaminated with amplified noise, if it can be found at all.

Equation (14) gives the least squares solution for an over-determined problem but it is only solvable if the product A^TA is invertible. This is not the case if, for example, some of the columns are not linearly independent. In this case the matrix is *rank deficient*, and no unique solution can be found.

Although in some cases the system matrix is *mathematically regular*, its spectral decomposition is such that the smallest eigenvalues are so small compared to the biggest ones that the solution becomes unstable, and it is not possible to find a solution starting with noisy data due to noise amplification. The matrix is said to be *ill-conditioned.*

The common technique to deal with ill-posed problems is *regularization* [2, 15, 16, 17]. It modifies the spectrum of the system matrix, diminishing the impact of the smallest *singular values* of the kernel matrix A on the solution. The singular values are defined as the square root of the eigenvalues of A^TA. In Inverse Theory it is useful to describe systems in terms of their Singular Value Decomposition (SVD) because it is usual to have non-square kernel matrices. See Appendix II for a detailed description of the impact of the singular values on the solution of inverse problems.

The effect of regularization is to stabilize and smooth the solution, particularly in the presence of data perturbations. For the equations proposed in this work, this becomes

important when the number of data points N is large. Given the dimensions of the surface features that are of interest in the lumber industry and the typical length of lumber boards, regularization is essential for practical measurements.

Regularization can also make a calculation possible in cases where rank-deficiency would otherwise prevent a solution from being achieved at all. This could occur in the case where having common factors in the distances between sensors is unavoidable, e.g. when sampling rate has to be changed but the sensors arrangement cannot be moved.

Several regularization techniques are known. Tikhonov regularization [15, 16] is the most commonly used.

The procedure involves modifying matrix $\boldsymbol{A}^T\boldsymbol{A}$ in equation (14) to penalize a certain measure of the recovered model. This requires some *a priori* information about the model and/or the data noise level. The penalty can be applied to the norm of the model (size), thereby creating a "small" solution, to the norm of the first or second derivatives of the model, respectively creating "flat" or "smooth" solutions or any kind of weighted combination of these. In particular, Tikhonov regularization minimizes a weighted combination of both data misfit and norm, transforming functional (12) in

$$\begin{aligned}\Phi^{TIKH}(f) &= \left\| A f - g^{obs} \right\|^2 + \\ &+ \beta\left(\alpha_{small} \left\| f \right\|^2 + \alpha_{flat} \left\| W_{flat}\, f \right\|^2 + \alpha_{smooth} \left\| W_{smooth}\, f \right\|^2 \right)\end{aligned} \tag{21}$$

where β is the *regularization parameter*, W are derivative operators that depend on the characteristic of the model to be penalized [2] based on *a priori* information available about the solution, and the α - parameters are weights for size, flatness and smoothness.

The weighted combination of data misfit and model size can be interpreted as a trade-off

solution between resolution and solution variance. As β increases, less importance is given to the accuracy in the data fitting but more control of the noise amplification is obtained.

Differentiating the regularized functional (21) with respect to $\boldsymbol{f}$ and setting the result equal to zero to find the $\boldsymbol{f}$ that makes it stationary yields:

$$(A^T A + \beta W^T W) f = A^T g^{obs} \tag{22}$$

which consists of the Normal Equations (14) with the addition of the regularization term. In this equation,

$$W^T W = \alpha_{small} I + \alpha_{flat} W_{flat}{}^T W_{flat} + \alpha_{smooth} W_{smooth}{}^T W_{smooth} \tag{23}$$

The weighting matrices represent the discrete first and second derivative operators applied to the model vector:

$$W_{flat} = \frac{1}{h}\begin{bmatrix} -1 & 1 & & & \\ & -1 & 1 & & \\ & & -1 & 1 & \\ & & & \cdots & \cdots \\ & & & & -1 \quad 1 \end{bmatrix}, \quad W_{flat} \in \Re^{M-1 \times M}$$

$$W_{smooth} = \frac{1}{h^2}\begin{bmatrix} 1 & -2 & 1 & & \\ & 1 & -2 & 1 & \\ & & \cdots & \cdots & \cdots \\ & & & 1 & -2 \quad 1 \end{bmatrix}, \quad W_{smooth} \in \Re^{M-2 \times M} \tag{24}$$

with discretization step h.

In general, a combination of smooth and flat models is a reasonable choice because they directly damp the oscillating effect of measurement noise, plus a smaller addition of small model to control the matrix condition and correct any overall shape deviation. If any piece of information about model characteristics is available, selective regularization could be used to

affect different parts of it. This is particularly important for the present case, because the SE have unknowns of different nature, namely shape and rigid motion.

The regularization parameter β modifies the diagonal terms of $\boldsymbol{A}^T\boldsymbol{A}$, damping the effect of the smallest eigenvalues of the matrix. The effect of this modification is that of filtering the highest frequencies out of the solution. A very good review of the filtering properties is given by Gulliksson and Wedin [18].

The choice of the optimal value for the regularization parameter is not trivial. The specialized literature describes a number of methods to find it [2, 19, 20], with more or less requirement of previous information about the noise or the solution.

One of the most commonly used methods is Morozov's Discrepancy Principle. It states that the optimal amount of regularization is the one that makes the data misfit $\| A f - g^{obs} \|$ equal to the data noise level. The idea behind it is that it is not useful to try to improve a fitting if the discrepancy is already smaller than the average error in the data. If a certain standard deviation σ_i is associated with each data point and if they are independent and Gaussian with zero mean, the optimum parameter β corresponds to the expected value of χ^2 for the data misfit equal to the size of the data space, N.

$$\chi^2 = \sum_{i=1}^{N} \left(\frac{\varepsilon_i}{\sigma_i} \right)^2 = \sum_{i=1}^{N} \left(\frac{g_i^{\,pred} - g_i^{\,obs}}{\sigma_i} \right)^2 = \sum_{i=1}^{N} \left(\frac{\sum_{j=1}^{M} A_{ij} f_j - g_i^{\,obs}}{\sigma_i} \right)^2 = N \qquad (25)$$

The product $\boldsymbol{A}\boldsymbol{f}$ is known as *predicted data.*

For the case where the standard deviations of all the misfit errors are the same, $\sigma_i = \sigma$ for all i, equation (25) reduces to:

$$\left[\frac{\left\| \boldsymbol{A}\boldsymbol{f} - \boldsymbol{g}^{obs} \right\|}{\sigma}\right]^2 = N \qquad (26)$$

Once an estimate of the standard error in the measured data, σ, has been made, equations (22) and (26) can be solved iteratively for β to achieve the desired misfit. The result is not sensitive to modest variations in β, so accurate convergence is not necessary. This tolerance is attractive because it could remove the need to evaluate β for every profile. For stable and consistent applications, it may be sufficient to use a fixed value of β that is updated only periodically.

3.11 Regularization examples

The features of the regularization procedure described above were examined by applying the process to two examples. The first feature of interest is smoothing a reconstruction of a model from noisy data. The unregularized reconstruction in Figure 9 (top bold) shows the adverse results of measurement noise. It is desired to use regularization to avoid noise fitting. Putting $\sigma = 0.1\ mm$ and iteratively solving equations (22) and (26) gives the regularized solution shown in Figure 9 (bottom bold). The trade-off between removal of data noise artifacts and loss of resolution is clear. The regularized profile is smoother, but at the expense of rounding the sharp corners at the steps. The role of regularization was to avoid data overfit and the procedure required some *a priori* information about the magnitude of contaminating noise. In this case, however, noise amplification was not too severe because the system was small. Regularization is essential when the number of data is large (in practice of the order of 500) due to the ill-posedness of the system matrix with increasing size.

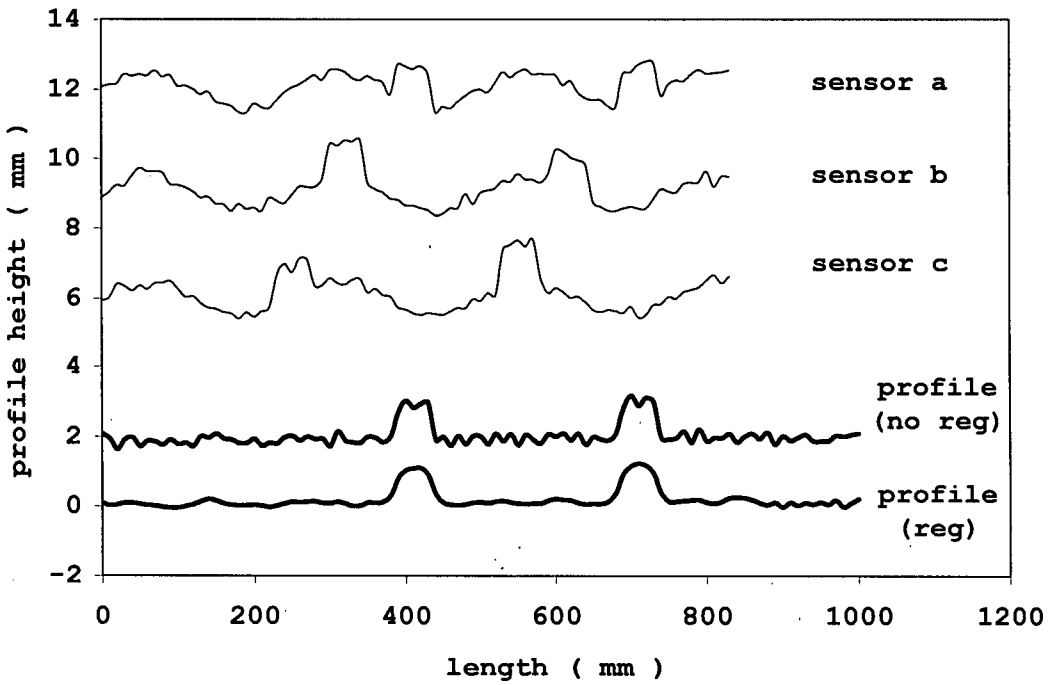

Figure 9 Smoothing effect of regularization for noisy data

The second regularization feature of interest is stabilization of an overdetermined system whose matrix is rank deficient in columns. This occurs when the numbers of data points between the sensors used in Figure 3 have common factors. To examine this case, sensor separations $p = 9$ and $q = 6$ were chosen. These numbers have a common factor, resulting in a matrix with null model eigenvectors. Regularization is essential because otherwise the system matrix in equation (14) is singular. Figure 10 shows the recovered solution. This singular situation is important in practice. For example, if the sample rate must be changed but it is inconvenient to rearrange the sensors position.

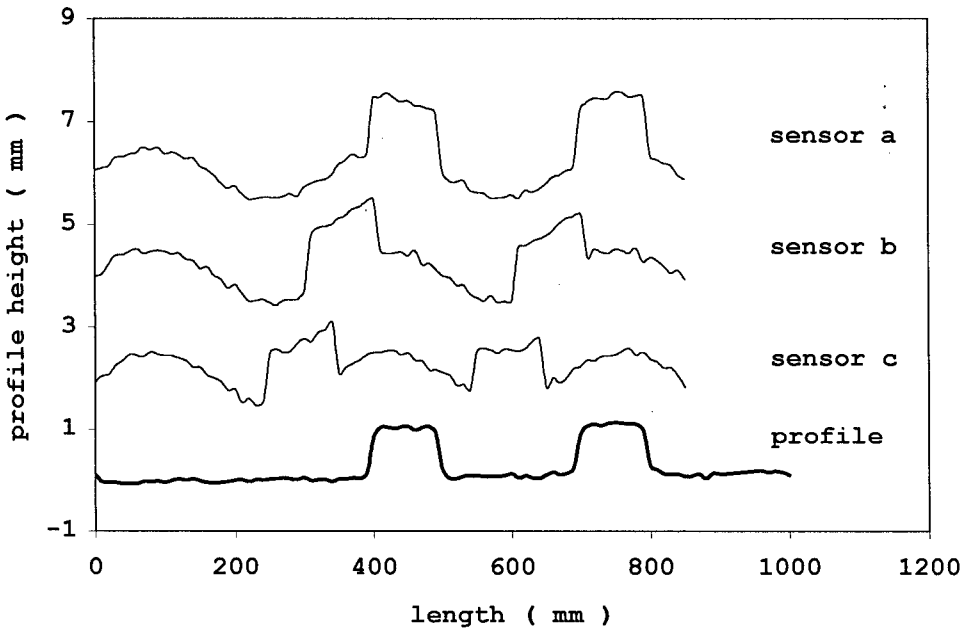

Figure 10 Regularization of singular systems

The effect of regularization was to exclude the null singular vectors from the inversion. However, the effect of some nonzero small singular values were also damped by the filtering effect of regularization, and some resolution is lost. This is because the singular vectors associated to the small singular values are those in charge of fitting the highest frequency components of the model.

CHAPTER 4. Experiment

4.1 Laboratory set-up

The practical effectiveness of the above profiling method was first tested using laboratory equipment similar to that shown schematically in Figure 1 for each of the cases already described (see Figure 11).

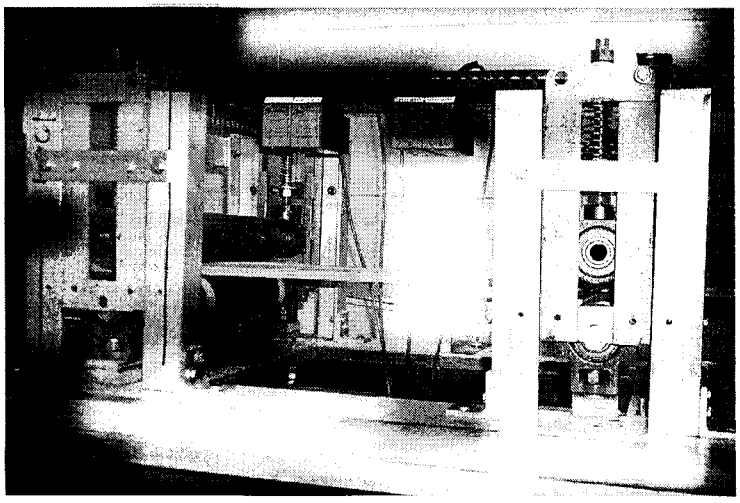

Figure 11 Experimental set-up for one-sided profiling with four sensors Board moves from right to left, and sensors are a-b-c-d from left to right

The boards traveled on the two bottom rollers, separated by *580mm.* Two top rollers held the piece by pushing it down against the bottom rollers. Lateral motion was minimized with mechanical constraints. The rollers were wrapped with sand paper. This was useful to avoid slippage between roller and board surface. A BEI® L25 incremental optical rotary encoder kept track of the longitudinal displacement of the board by measuring the angular position of the top right roller. See Appendix III for specifications.

The distances to the piece surfaces were measured with a set of laser sensors manufactured

by Hermary® Optoelectronics. The sensors measure distance to a surface by triangulation principle and they are widely used in the wood industry. The chosen model was the LRS-50, with a measurement range of *127mm – 1651mm* and a resolution of *0.05mm* in the short range. For applicability reasons, it is encouraging that they have already been extensively tested in the sawmill environment. Further details can be found in Appendix III.

The lasers and the encoder signals are combined in a *1kHz* signal concentrator, also manufactured by Hermary. A personal computer received the data from the concentrator via an Ethernet connection. A dedicated data acquisition code jointly developed at Forintek and UBC took the signal from the concentrator and organized it so that it could be fed into the solving algorithm.

4.2 Example cases

4.2.1 One-sided profiling

The first case of study corresponds to four lasers measuring only one side of a board. Four laser sensors were mounted in a row, at intervals *44mm*, *154mm* and *44mm*. This corresponds to $p = 2$, $q = 7$, $r = 2$, and a step size $h = 22mm$. A piece of wood, *1.5m* long and with a sinusoidally contoured upper surface was used as a specimen. An optical encoder attached to the right driven roller measured the longitudinal displacement of the specimen, and controlled the operation of the lasers so that they made their measurements at the desired length intervals. The decision to take range measurements upon request of the encoder signal was based on the fact that no assumption whatsoever can be made regarding feed speed constancy in a sawmill conveyor. This implies that readings are taken independently of time,

i.e. based on displacement. In this way, data points were equally spaced regardless of the feed speed. This corresponds to the use of x as a quasi-temporal variable in the SE.

To provide a significant amount of rigid-body motion with an otherwise accurate conveyor, a *4mm* high step was taped to the left roller. The specimen bounced over this step once per roller turn and the rigid motion had both translational and rotational components.

The first four traces in Figure 12 show the data acquired by each of the four sensors. They are irregular in shape, and clearly show the distortion introduced by the rigid-body motions from the stepped roller. The fifth trace shows the reconstructed surface calculated using equation (16). The rigid-body motions are successfully removed, and a smooth profile is observed. This profile locally agrees within *0.2mm* of the profile measured using a conventional profilometer with an accurate specimen traverse that did not introduce extraneous rigid-body motions, as can be seen in Figure 13. This figure shows a detail of the central portion of the profile from the previous calculation.

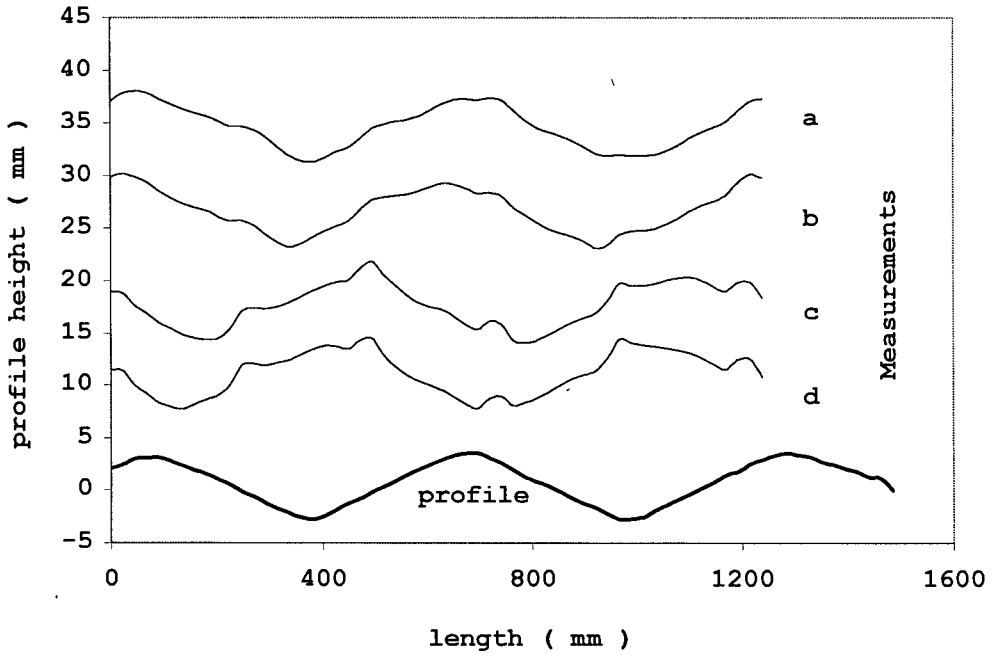

Figure 12 Experimental one-sided profiling

a, b, c, d are the four sensors signals. The recovered profile is shown at the bottom

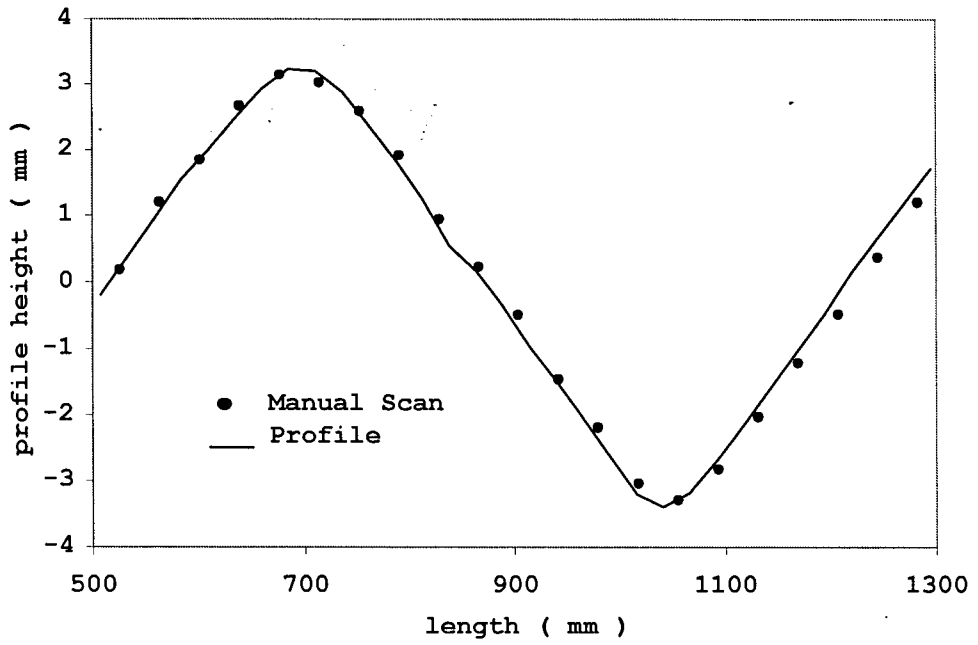

Figure 13 Validation of previous results using a precise surface scanner

Detail of central portion of bold profile in Figure 12

4.2.2 Two-sided profiling

The following experiment was carried out to illustrate the effectiveness of this sensor arrangement. The contoured piece of wood used for 4.2.1 was again used as a specimen. One surface had a sinusoidal shape, while the other was flat. The sinusoidal surface was loaded downwards in the roller conveyor schematically illustrated in Figure 6. Consequently, as the specimen moved forward, it also oscillated up and down. The step on the left roller was retained and provided additional rigid-body motion. The sensor spacings were *90mm* and *130mm*, with a step size of *10mm,* corresponding to $p = s = 13$ and $q = r = 9$.

Figure 14 shows the six sensor readings and the computed surface profiles. Signals from the three bottom sensors have been inverted for clarity. The profile distortions from the various rigid-body motions are readily apparent. However, the flat upper surface is accurately reproduced, and is distinct from the sinusoidal lower surface. The thickness of the specimen, as indicated by the difference between profiles in Figure 14 (bold line) agrees with independent caliper readings within *0.2mm*.

The "lower surface" profile in Figure 14 (lower bold line) corresponds to the profile in Figure 12. The inversion of the shape occurs because the specimen was turned upside down for the experiment in Figure 14.

The vertical motion due to the lower surface contour produces the long-wavelength pattern observed in the three bottom sensors signals. Rollers separation is approximately one contour wavelength. Therefore, there is substantially more rigid motion than before.

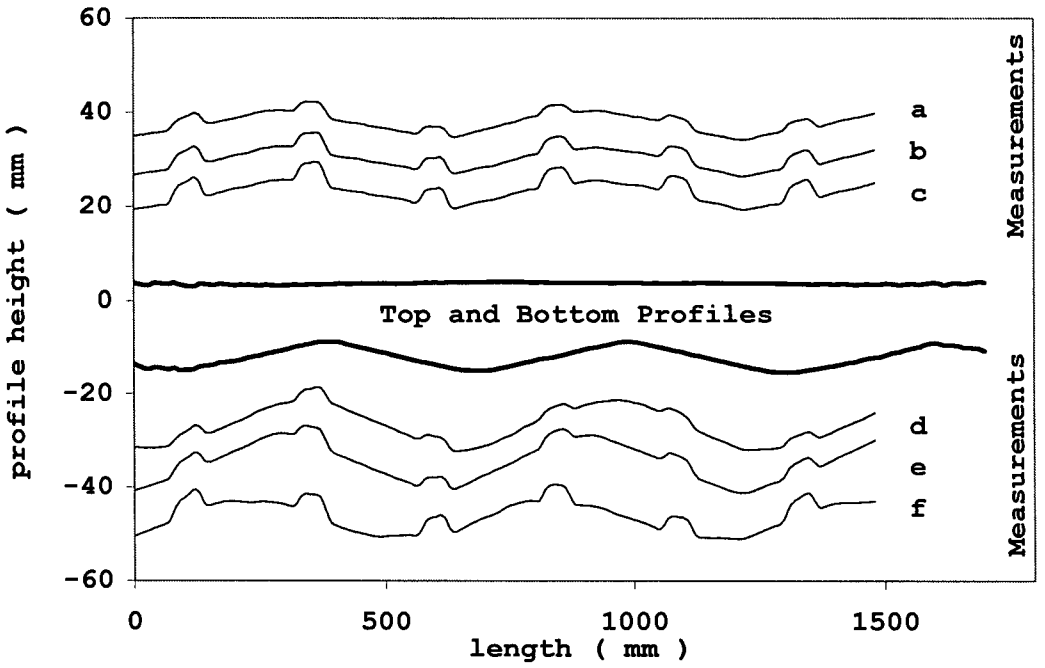

Figure 14 Two-sided profiling.

a to f are the six sensors signals. The top and bottom reconstructed profiles are shown in bold lines.

4.2.3 One-sided parallel profiling

An experiment was conducted to investigate parallel profile measurements using the sensor arrangement in Figure 7. A twisted piece of wood, *1.7m* long with uniform rectangular cross-section *235mm* × *38mm* (commercialized as 2" × 10"), was chosen as a specimen. The sensor spacings were *130mm* and *90mm* for the front line and *90mm* and *130mm* for the back line, with a step size of *10mm*. This gave $p = s = 13$ and $q = r = 9$.

The solid lines in Figure 15 show the computed surface profiles. For conceptual clarity, the starting heights of both reconstructed profiles are set equal to each other, and curves are rotated so that the front line starts and ends at the same height. The height difference between the two profiles corresponds to the specimen twist. The discrete points in Figure 15

correspond to independent measurements made manually using a height gauge with the immobilized specimen. The computed profiles agree well with these manual measurements. A source of discrepancy is specimen flexibility. The wood board that was used could significantly bend and twist under its own weight, depending on the way that it was supported. During the manual measurements, care was taken to support the board as similarly as possible to the way that it is supported in the conveyor.

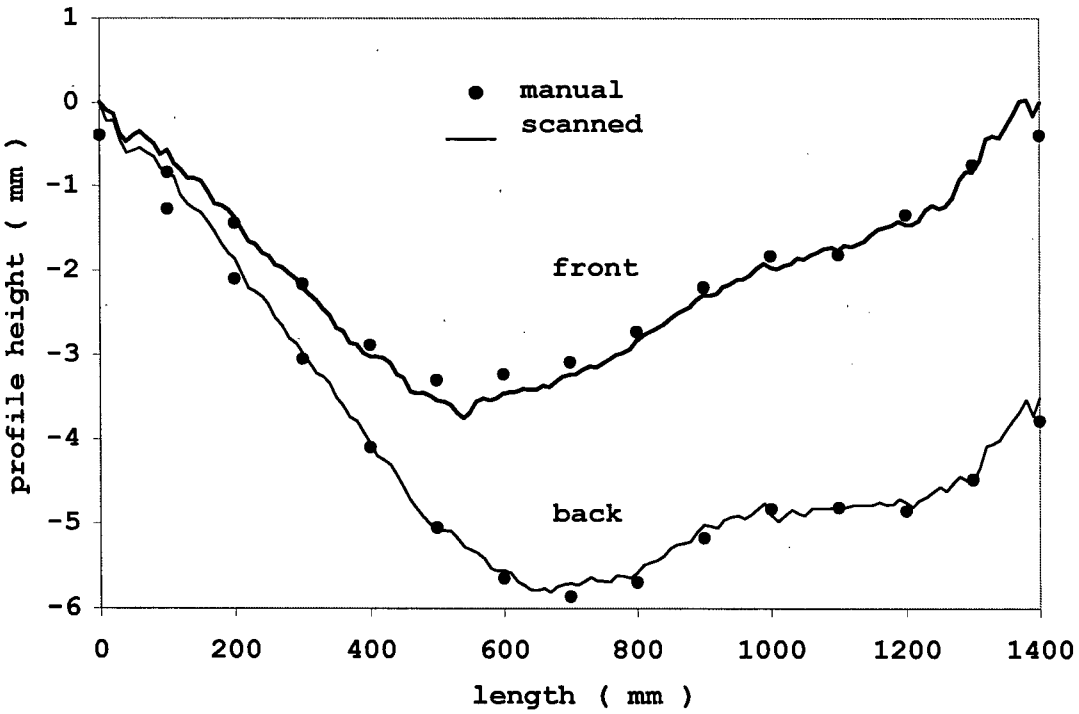

Figure 15 One-sided parallel profiling

Solid lines indicate calculated profiles. Dots are the result of Vernier measurement

4.2.4 Two-sided parallel profiling

The last case considered here illustrates measurement of a twisted specimen along four parallel lines, two on the upper surface and two on the lower surface. This measurement task requires use of at least eight sensors. Figure 8 shows the chosen configuration, with $p = s = 220mm$ and $q = r = 130mm$. To avoid system nulls with this minimal sensor arrangement, the sensors cannot occupy the corners of a rectangular arrangement analogous to Figure 6. As with the double-sided sensor arrangement in Figure 6, it is important for accurate thickness evaluation that at least two sensors along each pair of upper and lower profiles should oppose each other. The sensor arrangement in Figure 8 meets this requirement. The staggered arrangement of sensors creates surface profile reconstructions that differ slightly in length and start points.

The two pairs of lines in Figure 16 show the reconstructed upper and lower surface profiles. The thick lines refer to the front profiles and the thin lines to the back profiles. Noise contamination is slightly more apparent at the extremes of the reconstruction because these areas are scanned by only one sensor.

Overall sample twist could be defined as the average of the top twist and bottom twist:

$$TWIST_i = \frac{\left(u_i^F - u_i^B\right) + \left(v_i^F - v_i^B\right)}{2} \tag{27}$$

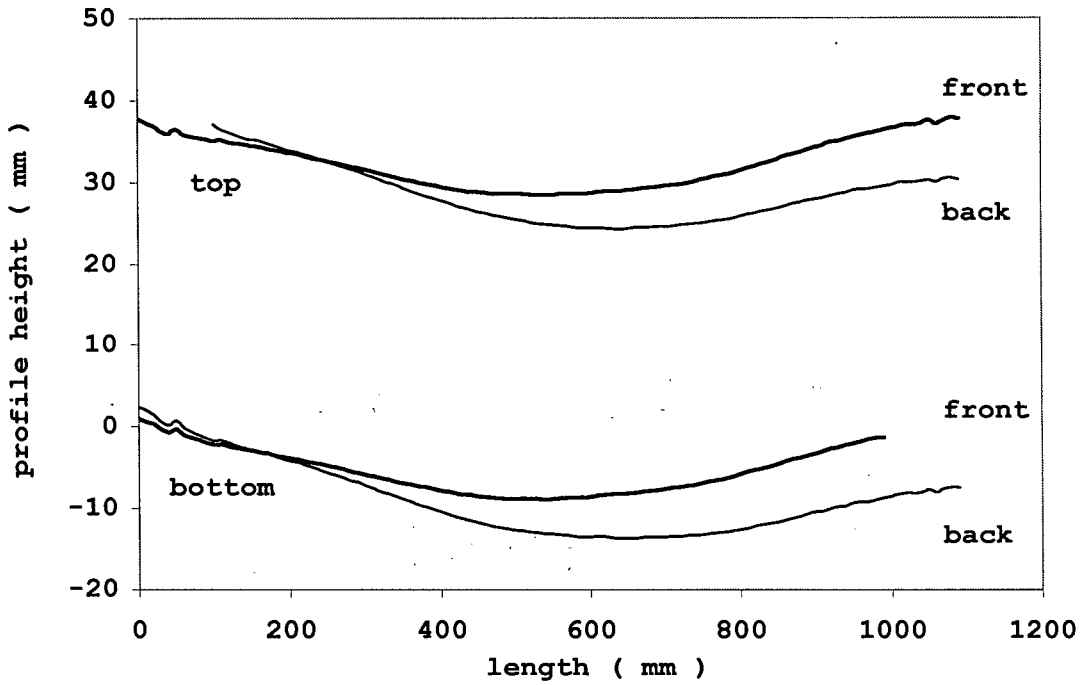

Figure 16 Two-sided parallel profiling

4.3 Omission of rotation

A parametric study of the condition number of the system matrix reveals that it increases linearly with the number of scanned points n if rotation is excluded from the equations (equation (8)) whereas the relationship is quadratic when rotation is present (equation (16)). The immediate question arising from this study is: Is it necessary to include rotation in the equations (at the expense of increasing the system instability and the computational effort), or are the results unaffected if its influence is neglected? The answer depends on the relative importance of z compared to the other variables. This is associated to the specimen rotation angle and the total span of the sensor array. The following experiment illustrates this statement. A very flat aluminum bar (*25mm* thick) was scanned using the sensor configuration of Figure 6. A *5mm* bump on one roller created the following pattern in the six

signals (bottom sensors signals are inverted for clarity):

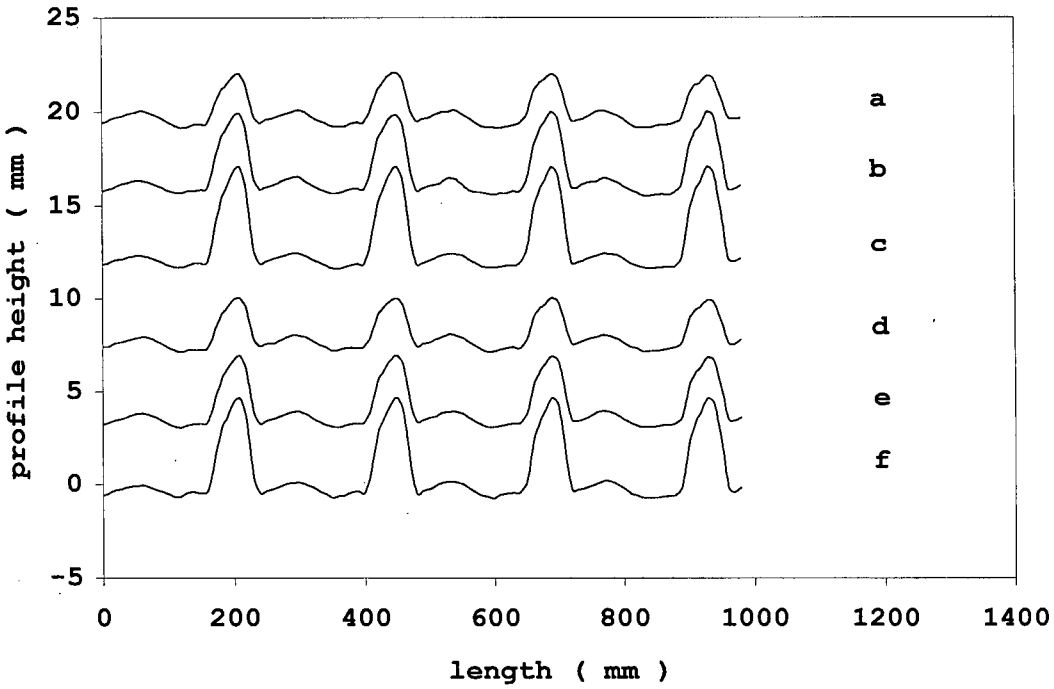

Figure 17 Sensor readings of two-sided profiling of a flat surface
Addition of a bump creates a repetitive roto-translational pattern that is detected simultaneously by all six sensors (a - f)

The rotational character of the rigid motion can be clearly identified when comparing the bump heights, increasing from ***a*** to ***c*** and from ***d*** to ***f*** according to the distance from each sensor to the bumped roller. Total rotation, with *580mm* of separation between rollers and *5mm* of step height, was *0.5°*. For the sensors configuration of the experiment, this corresponds to $z = 1.1mm$.

Figure 18 shows the surfaces reconstruction of the data without rotation (equation (8)) and with rotation (equation (16)). Thickness was reduced by *20mm* to permit better visualization of surface details. Clearly, not considering rotation creates severe reconstruction artifacts and the conclusion is that it must be included, even at the expense of increasing the matrix condition number.

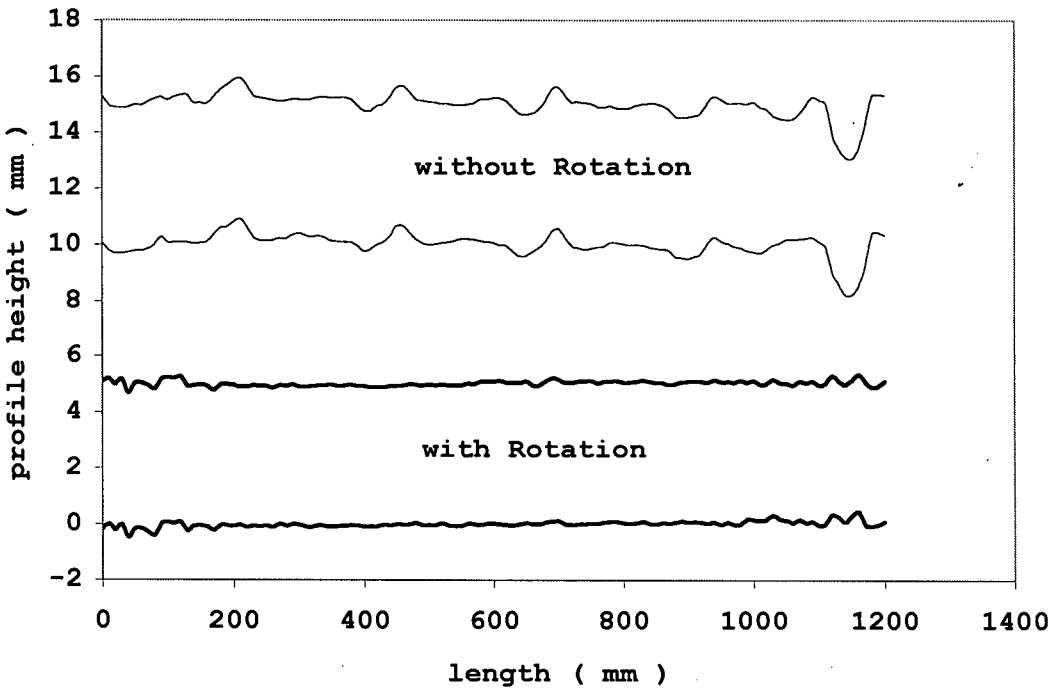

Figure 18 Surface reconstructions excluding and including rotation in the SE

4.4 Application to lumber profiling

4.4.1 Experimental set-up

The principal objective of the present work is to profile lumber boards on both sides independently, in real time and in presence of rigid body motion. In an attempt to better reproduce sawmill scanning conditions, a multiple roller conveyor was set up with the two-sided configuration of section 3.7. As it can be seen in Figure 19, the staggered double side arrangement is mounted to scan lumber passing through. This time, the encoder is attached to a long shaft that is engaged to all the rollers simultaneously through rubber belts. Sand paper was wrapped around the rollers to minimize slippage. The data acquisition scheme was modified such that the scan started as soon as all six sensors measured the wood surface. End of scan could either be triggered by the end of the board or by a fixed scan length.

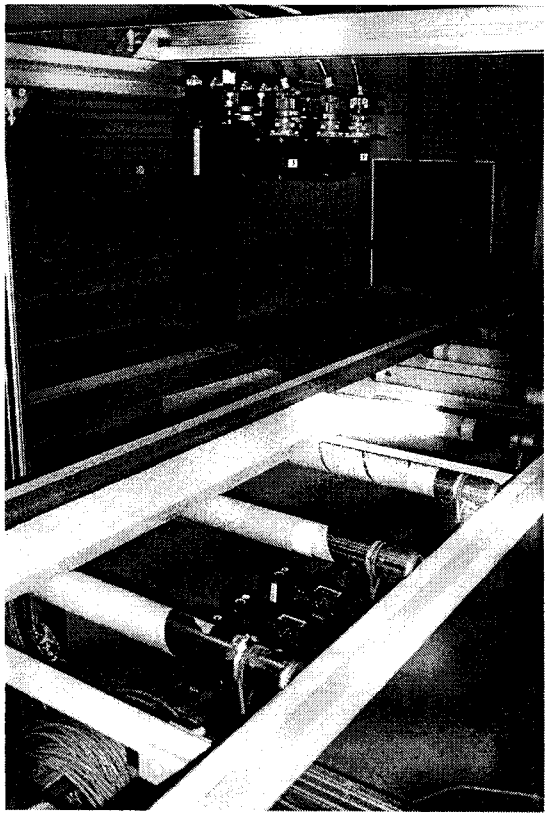

Figure 19 Multi-roller conveyor. Six sensors – Two sides set-up

The geometry of the set-up was decided based upon typical scanning parameters for industrial lumber boards, mechanical and physical conditions of cutting and product handling.

Board Length (**L**)	**2700mm**
Sample Spacing (**h**)	**3mm**
# of Surface Points **n** = 1 + L / h	**901**
Sensors spacing [**p , q , r , s**]	**[43 , 30 , 30 , 43]**
# Points per sensor (**ndata**) = n – (p + q)	**828**
# Sensors (**ns**)	**6**
# Total Data Points (**N**) = ns × ndata	**4968**

4.4.2 Computational considerations

Referring back to equations (17) the system will be characterized by a matrix A of dimensions 4968 × 3456. Therefore, the number of elements in the least squares matrix is almost *12 million.* But it also can be shown that the number of *nonzero* elements will only be of the order of *1%.* Moreover, its columns can be reordered so that it becomes banded, with a bandwidth related to the distance D. All these features make the system suitable to be solved with a specialized routine [21] that exploits the banded structure and symmetry (storing half the band), saving memory and computational time by neither storing nor multiplying zeroes.

Regularization is essential because the condition number of the resulting matrix is of the order of 1.5×10^7. Otherwise, noise amplification would make the results useless.

4.4.3 Real lumber tool marks

The next subsections (4.4.3.1 to 4.4.3.4) show examples of profile calculation of boards surfaces with features that are of industrial interest, linked to sawing deficiencies.

An expert system is currently being developed at Forintek Canada, whose objective is to identify tool marks from these results.

In the corresponding figures, left and right vertical axes values represent top and bottom height profiles respectively, in order to show the board surface more effectively.

4.4.3.1 Saw runout

Deviation from flatness causes the cutting edge of a circular saw to move laterally during sawing. This generates an oscillatory pattern on the wood surface whose wavelength equals the length of wood cut during one revolution of the saw. The upper profile in Figure 20 shows the surface profile of a piece of lumber which was cut with a circular head saw, *914.4mm* (*36"*) diameter, with a feed per revolution of *100mm*.

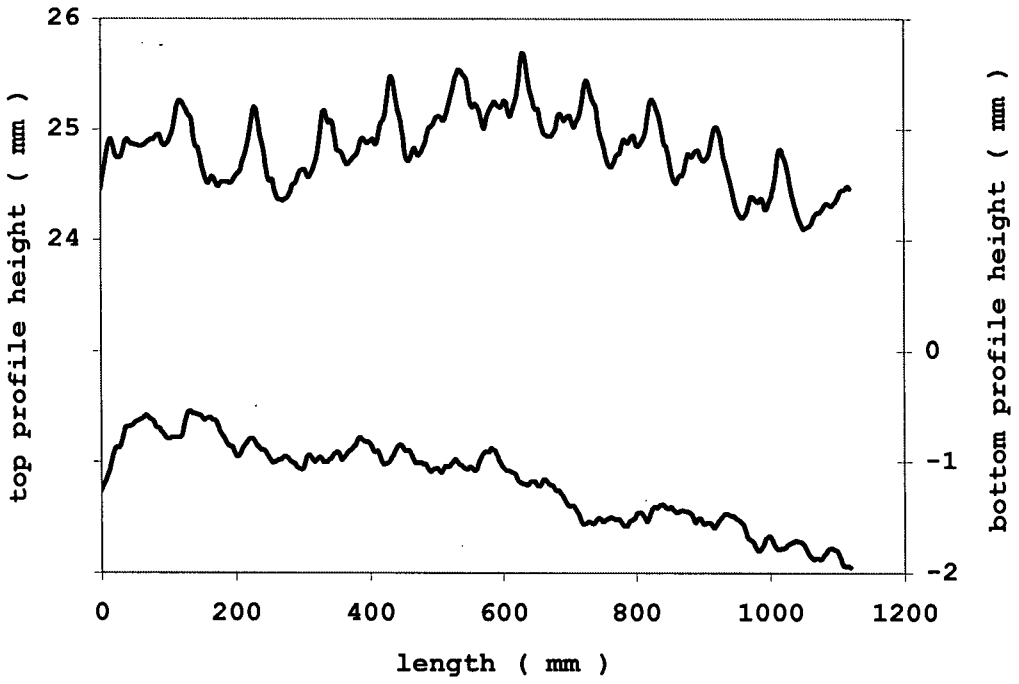

Figure 20 Runout pattern caused by a circular saw on top surface

4.4.3.2 Knot tear-out

The tear-out, a common defect created by chipping heads in the vicinity of knots, is a hole caused by the action of the tool in zones where fibres direction and wood strength change substantially. A knot tear-out can be appreciated on the bottom surface in Figure 21 on a board. On the top surface, a small repetitive bump, probably caused by a missing tooth of the band-saw, is observed every *200mm*. This is a good example of pattern identification in lumber boards that have been cut by different tools on each side. The proposed method allowed separate visualization of the two independent defects.

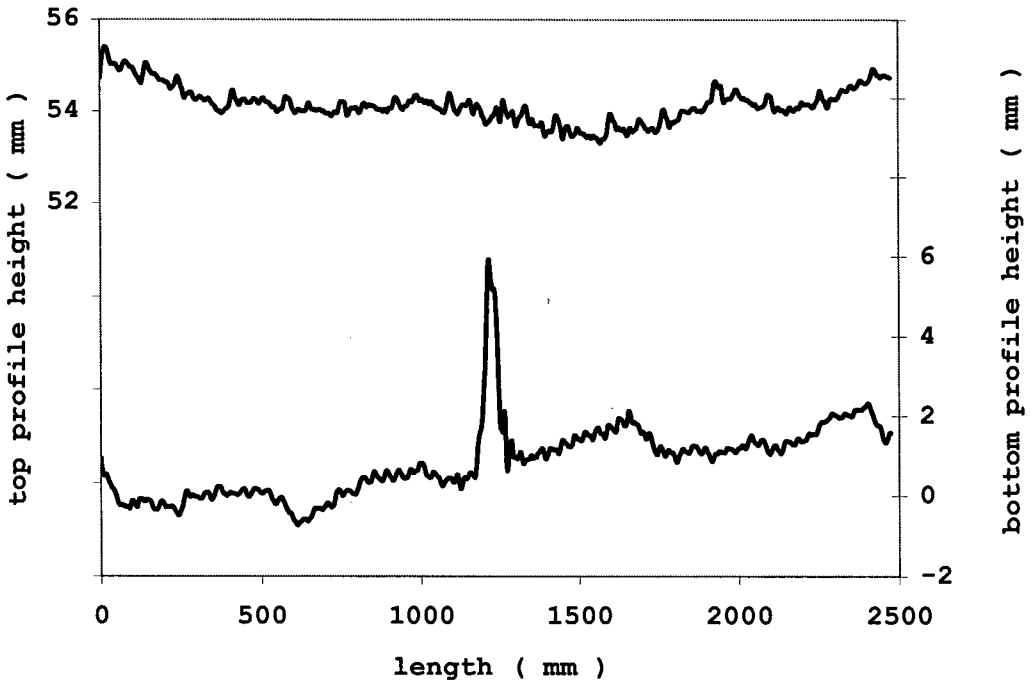

Figure 21 Knot tear-out on the bottom surface

4.4.3.3 Washboard

This characteristic pattern is observed in both circular and band saws and is related to abnormal vibration of the blade due to its interaction with the wood piece. Washboard is characterized by a sinusoidal undulation with an amplitude of about *0.5* to *1mm*. Figure 22 shows an example of the pattern produced by a band saw on both sides of the piece. Notice the characteristic sinusoidal pattern. A small knot tear-out is also present on the bottom surface.

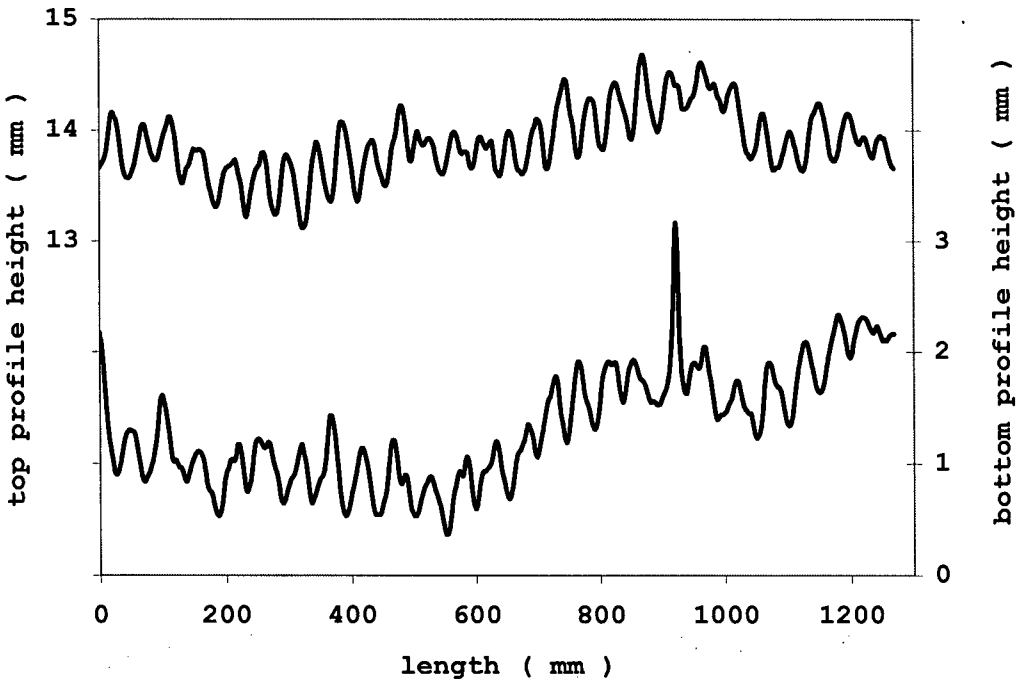

Figure 22 Band saw washboard pattern on both sides
A missing knot is observed on bottom surface (≈920mm)

4.4.3.4 Scallop

A further periodic pattern created by chipping heads is the scallop surface. Its characteristic pattern is similar to that of washboard, sinusoidal shape with slightly sharpened tops corresponding to the boundaries between successive scallops. The top surface in Figure 23 shows a scallop pattern of increasing severity, whereas its bottom surface does not present any noticeable defect.

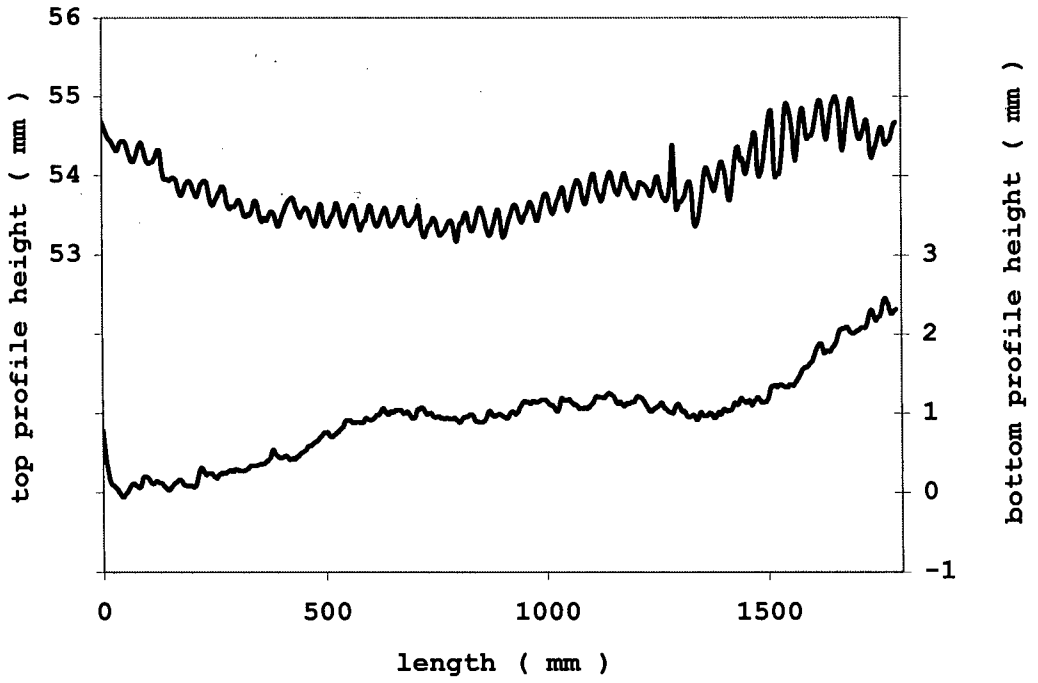

Figure 23 Scallop pattern on top surface

4.5 Sources of errors and artifacts

This section describes the effects of different sources of measurement errors on surface evaluation accuracy. They correspond to assumptions implied in the SE that are not fully accomplished.

4.5.1 Deviation from scan lines

The proposed measurement method relies upon the fact that the laser arrays scan along lines on the surface and therefore each laser sees the same set of points. However, this is unlikely to happen in practice due to unavoidable imperfections of the conveying device. The laser array will not describe a straight line and a given sensor will not see the same point that was spotted by its neighbours. The outcome of this type of situation can either be serious or harmless depending on the rate of variation of surface pattern across the surface width. Fortunately, many surface patterns of practical interest (such as washboard, bent tooth, large knot tear-out and snaking) only have a small lateral gradient and the error due to lateral movement can be neglected. Other features (e.g. small knot tear-outs) could be missed by some sensors if the lateral movement occurs while the defect is within the sensor array span. The result is a surface artifact created by the algorithm in an attempt to reconstruct a model to fit the unrealistic data. This artifact usually causes distortions on the shape of the surface in the vicinity of the mentioned feature.

The following experiment shows an example of the system response in a case like the aforementioned. A *8mm* high, *12mm* long object was placed on top of the surface of a quite flat board with the two-sided configuration of Figure 6. The object was scanned by sensors ***c***

and ***b***, but before arriving to sensor ***a*** it was removed from the surface. Only two out of three sensors detected its presence.

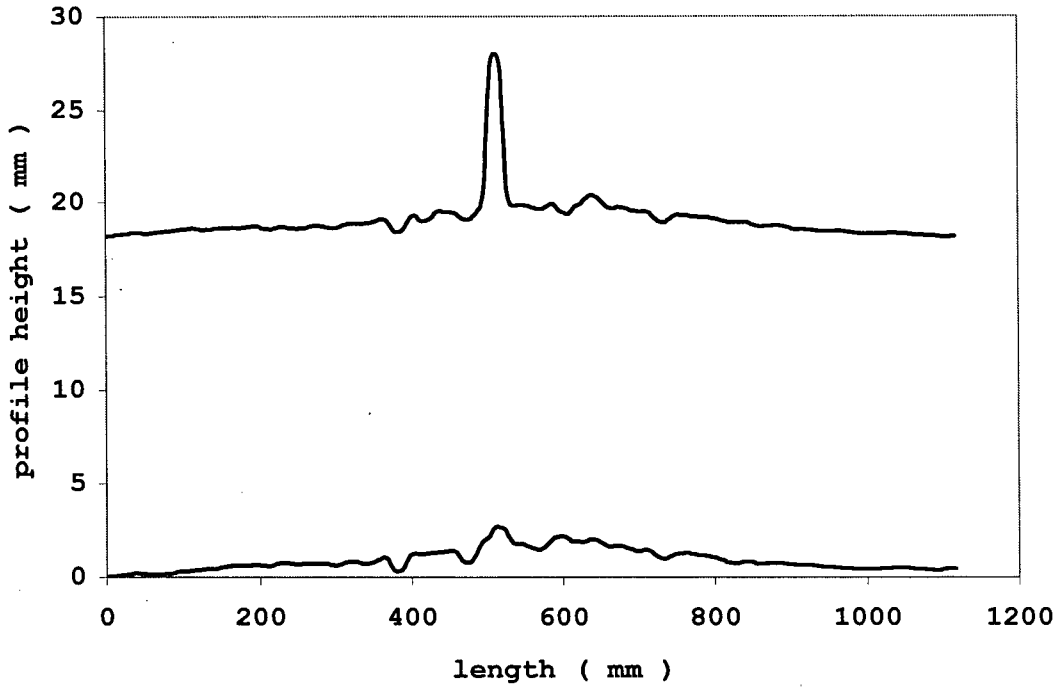

Figure 24 An object that is seen by only two of the three top sensors creates a smearing artifact

Figure 24 shows the reconstruction of the two surfaces. What should have appeared as a clean isolated protuberance is in fact surrounded by spurious artifacts. Interestingly, the contamination also affects the bottom surface, although to a lesser extent.

Even when the result is not a truthful reconstruction of the surface shape, it is not useless for pattern detection purposes because the presence of an unusual feature is not ultimately overlooked.

4.5.2 Vibration and bending

The mathematical formulation of the present method considers that the acquired signal is a superposition of a height profile and a rigid motion. Rigidity, of course, is a practical assumption whose validity depends on the sample characteristics: elastic constant, length, cross section shape, etc. Depending on their magnitudes and on the mechanical and physical conditions of the transport system, a non-negligible flexural vibration can also contribute to the signal composition.

Bending recognition constitutes a limitation of the measurement method as a whole, for it is not possible to distinguish it from a real long wavelength overall shape. Nevertheless, most patterns of practical interest have wavelengths far smaller than those characteristic of bending, with the possible exception of very long snaking. Keeping in mind that excessively rough patterns are ultimately shaved out in a planer and that this machine straightens the lumber pieces while machining, this limitation concerning very long wavelength features does not constitute a serious drawback.

Flexible vibration, however, introduces a spurious sinusoidal pattern in the surface calculation that should not be confused with real surface shape. Fortunately, it is not difficult to classify such spurious result as an artifact. The recommended procedure for assessing a suspicious case involves looking at a similar pattern in the reconstruction of the rigid motion. If the same sinusoidal pattern is observed in the rigid motion as well, there is almost no doubt that the signal is affected by a vibration artifact, for it is highly unlikely to have such similarities between the two reconstructions.

There is a trade-off in the choice of the total length spanned by the sensors array, because

flexible vibration artifacts are more likely to appear for long spans, whereas short spans are prone not to identify long wavelengths correctly.

The following experiment, although contrived and exaggerated, illustrates the consequences of submitting a very long and flexible *20mm* thick board to first mode vibration of *5mm / 10mm* of amplitude, using the same experimental configuration as before. Four hundred millimeters after the scanning had started, the tip of the board was lifted and moved up and down to make the board vibrate along its entire length. Figure 25 shows the resulting profile reconstruction, where *15mm* of thickness were removed from the graph to clearly show the surface pattern (bold lines). A *0.6mm* spurious oscillation contaminates the surface reconstruction. The reason for this is that the amount of bending curvature is excessive for the oscillation to be considered rigid.

However, this pattern can easily be identified as an artifact, because a sinusoidal pattern of the same frequency appears in the rigid motion calculation (top graph).

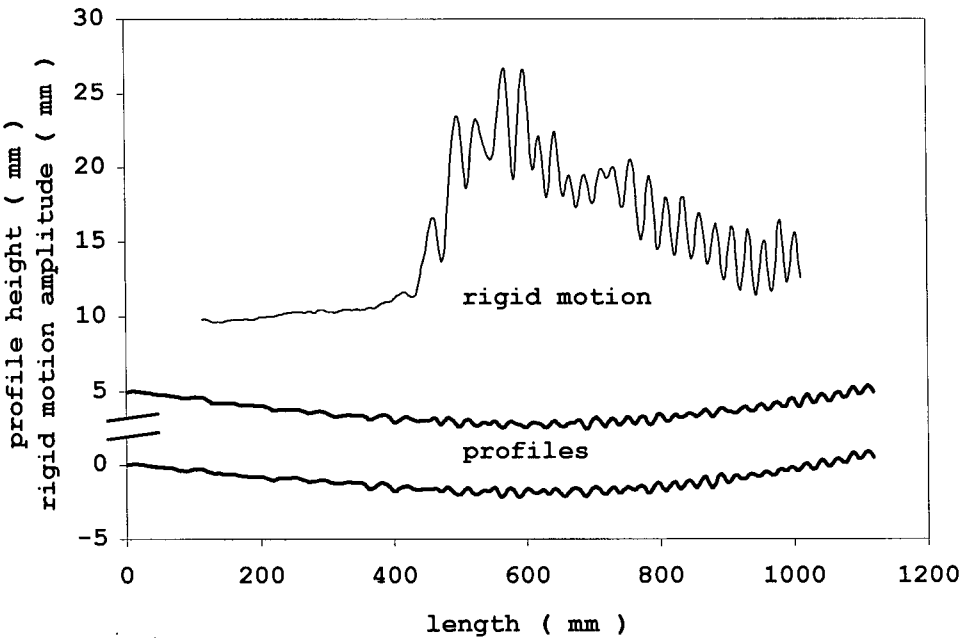

Figure 25 Oscillatory artifact created by bending vibration

4.5.3 Erroneous measurement of longitudinal displacement

The advantage of profiling independently of longitudinal velocity of the board (section 4.2.1) is associated with an important mechanical requirement: displacement has to be measured accurately. Possible sources of discrepancy in this respect are those related to slippage between the conveyor and the board. Once more, this is very unlikely to happen at early stages in the sawmill because of the weight of the pieces and due to the fact that the transportation is achieved via a nailed chain. However, as the scanned pieces are smaller, some relative displacement between the conveyor and the lumber board could be expected. In an attempt to visualize the possible erroneous reconstruction of the surfaces, let us consider the example described in section 4.4.3.3. An easy way to simulate a constant slippage along the entire scan is to re-invert the same data, artificially setting a false distance between sensors. Increasing the values of *p, q, r* and *s* given in 4.4.1 by ten percent, the surface profiles are:

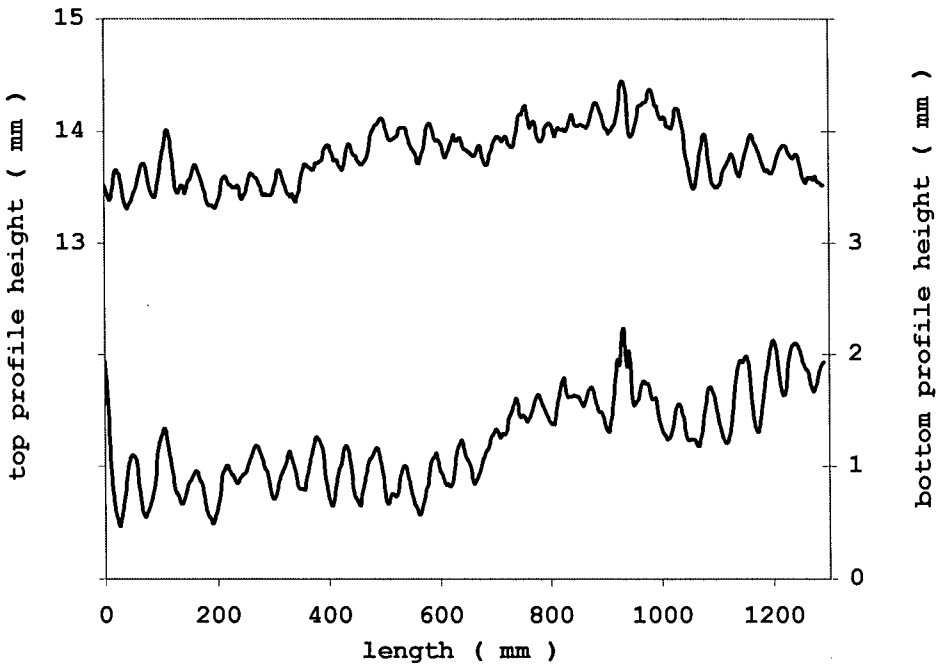

Figure 26 Slippage error

A sinusoidal pattern can still be recognized, but details are distorted.

In general, it can be seen that violations to the essential SE assumptions create artifacts and distorted reconstruction. However, the presence of abnormal surface patterns is not overlooked and the system output could be used to make the scanned piece a candidate for subsequent manual analysis.

4.6 Progressive solution

The banded structure of the least squares matrix and the physics of the problem itself suggest the existence of some independence of the surface profile within a region on the data acquired away from it. This idea should be useful in an attempt to solve the SE in a recursive way. That is, given some estimation of the initial value of the unknowns, to construct an iterative algorithm that solves for the surface profile points based only on the data acquired in its vicinity.

Although some numerical experimentation was made in an attempt to develop this attractive alternative, the results were not satisfactory. The recursive equations resulting from the algebraic manipulation of the SE were found to be non-convergent. Details about this idea can be found in Appendix IV.

CHAPTER 5. Conclusions

5.1 Summary of results

The results described in the present work show that the sequential measurements approach to moving surfaces profiling is a promising alternative to existing methods.

The proposed equations permit surface reconstruction of both sides of long flat objects independently along single or multiple lines. Rigid-body motion can be successfully removed from the sensors signals. Unlike thickness measurement, this method reconstructs top and bottom surfaces individually. Within the frame of lumber manufacturing control, this constitutes a substantial improvement. Independent information on both sides of the product can be directly linked to defective machining on a tool-by-tool basis. Consequently, this could potentially be used as input to an integrated maintenance system, where early detection and correction of failures leads to a better utilization of wood as raw material.

The proposed system is capable of reconstructing real surface patterns related to lumber cutting operative conditions.

The Sequential Equations were solved using inverse methods. The least-squares approach proved to be effective for relatively small problems, when data noise was not excessively large and the system was non-singular.

A large number of sample points causes excessively large noise amplification due to the inherent ill-posedness of the Sequential Equations. The Tikhonov regularization technique successfully stabilized the equations and also provided a solution for singular systems. The amount of regularization was chosen based on the discrepancy principle. The results were

observed not to be highly dependent on the regularization parameter. This result is encouraging for industrial purposes because it shows that the regularization parameter does not have to be calculated on a board-by-board basis, but can be chosen for a set and adjusted periodically if necessary.

Computational implementation in MATLAB was appropriate for small systems, but a dedicated FORTRAN routine had to be used for larger numbers of surface points, taking advantage of the symmetric banded structure of the re-ordered least squares matrix.

Experimental work on a laboratory conveyor shows that the system can readily be implemented using off-the-shelf laser range sensors, provided their sample rate capabilities match the longitudinal resolution required for a given specific application. Based on these results it is expected that the system can potentially be installed at any place in a sawmill where the pieces move longitudinally. For failure detection applications, however, the chosen place should be such that permits the user to identify the tools that cut a sample while it is being scanned.

Sensors should be placed as close to the surface(s) as possible to take advantage of the highest resolution range and minimize the possibility of laser spot displacement due to vibration-induced rotation of the sensors' frame.

Practical limitations of the method include the impossibility to differentiate bending curvature from actual shape curvature. This may not constitute a problem, especially if the system is installed at early stages in the sawmill, where either the sawn product is large enough so that bending is negligible, or the array is mounted horizontally and gravity does not affect the shape in the direction of measurement. However, when scanning long thin pieces, an overall curvature might appear due to uneven conveyor roll support.

Furthermore, reconstruction errors appear when the intrinsic assumptions of the method are not fulfilled: presence of flexural vibration of the scanned piece, deviation from the scan line and incorrect displacement tracking. Even when in these cases the obtained profile is not accurate, the presence of defects in the surface pattern is not ignored, and the user can still identify a problem or plan a re-inspection of the suspicious pieces.

The practical application described in this work was related to lumber scanning, but the system could potentially be implemented in other types of areas where two-sided long flat objects have to be profiled in presence of rigid motion or for short-wavelength surface profiling of railways and roads.

5.2 Future work

A very interesting application stemming from the results of the present work would be multi-line and 2-D scanning. Provided mathematical and computational techniques are developed to handle a bigger amount of data per board, the delayed-simultaneous scanning concept could be applied to a multiple line scanning system. Once the rigid body motion of the surface is calculated using a minimum number of sensors, additional sensors could be added at different locations and their profiles would result of the acquired data minus the rigid motion.

The banded structure of the reordered matrix (equation (15)) is related to some independence of the reconstructed profile on a given area on data acquired away from it. This suggests the possibility to write the SE recursively and solve them as a system of recursive equations. However, this is not possible in the way they are written at the moment, for they constitute a system whose convergence cannot be guaranteed.

References

[1] Kuenzi, T. "The effects of wane allowance, kerf and target size reduction on sawmill optimization". *Senior Project Report.* Department of Wood Science & Engineering, Oregon State University. June 2002.

[2] Menke, W. "Geophysical Data Analysis: Discrete Inverse Theory". *International Geophysics Series.* Vol. 45, 1989.

[3] El-Sibaie, M., Jamieson, D., Mee, B., Whitten, B., Kesler, K., Tyrell, D., Dorsey, J. "Engineering Studies in Support of the Development of High-Speed Track Geometry Specifications." *IEEE/ASME Joint Railroad Conference*, Boston. 8pp. March 18-20, 1997.

[4] Grassie, S. "Measurement of railhead longitudinal profiles: a comparison of different techniques." *Wear*, Vol.191, pp.245-251, 1996.

[5] Cooper, J. "Rail Corrugation Measurement." *Proceedings of "Rail Technology",* Nottingham, UK. (eds. C. O. Frederick and D. J. Round). pp.207-223. September 21-29, 1981.

[6] Hudson, W. "High speed road profile equipment evaluation." *Highway Research Record.* National Research Council, Highway Research Board. Vol. 189. pp. 150-165. 1967.

[7] Darlington, J. "A progress report on the evaluation and application study of the General Motors Rapid Travel Road Profilometer." *Highway Research Record.* National Research Council, Highway Research Board. Vol. 214. pp. 50-67. 1968.

[8] Wong, D., Schajer, G. Personal communication.

[9] Maness, T. Lin, Y. "The influence of sawkerf and target size reductions on sawmill revenue and volume recovery". *Forest Products Journal.* Vol. 45 No. 11/12 pp. 43-50. 1995.

[10] Takeshita, K. "A method for track irregularity inspection by asymmetrical chord offset method". *Quarterly Report of RTRI.* Railway Technical Research Institute. Vol. 33 No. 2. pp. 106-114. 1992.

[11] Buhler, F. "Measurement of undulatory wear along railroad tracks." *US Patent 4 075 888.* US Patent and Trademark Office, Washington, 1978.

[12] Corbin, J. "Method and apparatus for measuring surface roughness." *US Patent 4 573 131.* US Patent and Trademark Office, Washington, 1986.

[13] Yazawa, E., Takeshita, K. "Development of measurement device of track irregularity using inertial mid-chord offset method". *Quarterly Report of RTRI.* Railway Technical Research Institute. Vol. 43 No. 3. pp. 125-130. 2002.

[14] Eisenstat, S. C., Gursky, M. C., Schultz, M. H. and Sherman, A. H. "Yale Sparse Matrix Package. I: The Symmetric Codes". *International Journal of Numerical Methods in Engineering.* Vol.18, pp.1145-1151, 1982.

[15] Tikhonov, A., Goncharsky, A., Stepanov, V., Yagola, A. "Numerical Methods for the Solution of Ill-Posed Problems." Kluwer, Dordrecht, 1995.

[16] Tikhonov, A., Arsenin, V. "Solutions of ill-posed problems". John Wiley & Sons, Washington, D. C. 1977.

[17] Scales, J., Smith, M., Treitel, S. "Introductory Geophysical Inverse Theory." *Samizdat Press*. Center for Wave Phenomena. Dept. Geophysics, Colorado School of Mines, 2001.

[18] Gulliksson, M., Wedin, P. "The Use and Properties of Tikhonov Filter Matrices." SIAM J. Matr. Anal. Appl., Vol. 22 No. 1, pp 276-281, June 2000.

[19] Tikhonov, A., Goncharsky, A. (Editors). "Ill posed problems in the natural sciences." *Advances in Science and Technology in the USSR*. MIR publications, Moscow. 1987.

[20] Golub, G., Heath, M., Wahba, G., "Generalized cross validation as a method for choosing a good ridge parameter." *Technometrics*, Vol. 21, No. 2, May 1979.

[21] Anderson, E. *et al.* "Lapack User's Guide". SIAM, Philadelphia, 1992.

Appendix I. Minimum number of sensors required

Let us consider the general case of ***ns*** sensors profiling one or two surfaces along single or parallel lines. Defining the variables ***r***, ***h*** and ***k*** such that:

r = 0 if rotation is not considered

r = 1 if rotation is considered

h = 0 if profiling is single sided

h = 1 if profiling is double sided

k = 0 if the number of lines per side is one

k = 1 if the number of lines per side is two

The dimensions of the general kernel matrix will be

$$\#rows = \#data = ns(n-D)$$
$$\#columns = \#unknowns = n(1+h+k+hk)+(n-D-1)(1+r+k)$$

where D is the distance between first and last sensor.

In order to have a determined system, the number of data must be greater or equal than the number of unknowns:

$$ns(n-D) \geq n(1+h+k+hk)+(n-D-1)(1+r+k)$$

Then, for $n-D >> 1$

$$ns \geq \frac{n(1+h+k+hk)+(n-D-1)(1+r+k)}{(n-D)} \cong \frac{n(1+h+k+hk)}{(n-D)}+(1+r+k)$$

Equation that only has physical meaning for $(n > D)$ and that can only have integer values. It

follows that the first integer to accomplish with the inequality is

$$ns = 3 + r + h + 2k + hk$$

This means that there must be a minimum number of sensors equal to the number of unknown variables ($2 + r + h + 2k + hk$) plus one.

The same result is achieved even if the scanning starts and stops when only a partial number of sensors is measuring the surface, provided that the minimum number of sensors at any time is at least equal to the number of unknown variables.

Appendix II. Influence of singular values on noisy data inversion

Any $N \times M$ matrix can be decomposed as the product of three matrices:

$$A = U \Lambda V^T$$

where U ($N \times N$) and V ($M \times M$) are orthonormal matrices (called left and right singular vectors) and Λ ($N \times M$) only has nonzero elements in the main diagonal equal to the square roots of the eigenvalues of $\boldsymbol{A^T A}$.

For the case in study, $N > M$ and then A can also be written as

$$A = U_p \Lambda_p V_p^T$$

with $P = rank(A)$. Now U_P has dimensions ($N \times P$), V_p has dimensions ($P \times M$) and Λ_P has dimensions ($P \times P$). If there are no null model vectors, $P = M$. U_P and V_P columns are still orthonormal vectors.

Having decomposed the rectangular, full rank in columns, matrix A, its generalized inverse can be defined as:

$$A^{\dagger} = V_p \Lambda_p^{-1} U_p^T$$

where the dagger † symbol is used to emphasize that this is not an ordinary inverse because A is not square. It can be shown that this inverse corresponds to the least squares solution expressed in equation (14).

$$f_{LS} = A^{\dagger}\, g^{obs} = V_p\, \Lambda_p^{-1}\, U_p^{T}\, g^{obs}$$

Writing this in summation form

$$f_{LS} = \sum_{i=1}^{p} \frac{\left(u_i^{T} \cdot g_i^{obs}\right)}{\lambda_i} v_i$$

where u_i, v_i are the column vectors of U_P and V_P and λ_i are the diagonal entries of Λ_P.

And, writing an explicit term for the data noise:

$$f_{LS} = \sum_{i=1}^{p} \frac{\left(u_i^{T} \cdot \left(g_i^{obs} + \delta\right)\right)}{\lambda_i} v_i = \sum_{i=1}^{p} \frac{\left(u_i^{T} \cdot g_i^{obs}\right)}{\lambda_i} v_i + \sum_{i=1}^{p} \frac{\left(u_i^{T} \cdot \delta\right)}{\lambda_i} v_i$$

From this equation it is not difficult to see the detrimental effect of the very small singular values λ_i, amplifying the second (error) term of the summation.

Appendix III. Lasers and encoder specifications.

Laser Sensors

The choice of off-the-shelf triangulation sensors was made based on resolution and reliability. The Hermary LRS-50 is a widely used sensor in sawmills and other industries.

Principle of operation	Laser triangulation / CCD detector
Range of operation	127mm to 1651mm
Resolution (near range)	±0.05mm
Resolution (far range)	±1.7mm
Scan rate	1000 / sec
Serial interface	RS422

A signal concentrator Hermary LRS-16 HC gets the data from multiple sensors and transmits them to a PC via a 10MBit Ethernet AUI Port.

Calibration

Accurate calibration of the distances between sensors yields a trustworthy detection of high frequency changes in the surface by ensuring that all the sensors take measurements at the same places. On the other hand, calibration of the distances to the surface is related to the accuracy with which the system is capable of reproducing long wavelengths without overall curvature errors.

Calibration of the distances between sensors is satisfactorily done using a ruler, with an accuracy of *1mm*.

Calibration of the distances to the surface is achieved by taking range measurements of a very flat piece, storing the measured distances as references (i.e. H in section 3.2), and

correcting every subsequent measurement with these reference values. This adjustment is performed internally in the data acquisition program. Distance calibration prevents curvature errors. This is especially important when the sensors span length D is small, because an alignment offset of the sensor array is amplified quadratically with the scanning length:

$$\delta_{TOTAL} \cong \frac{L^2}{D^2} \times offset$$

As an example, consider the case explained in 4.2.2, where $D = 220mm$, $L = 2400mm$ and an offset of the order of the sensor resolution $\sigma \approx 0.05mm$. Total deflection due to curvature error is expected to be:

$$\delta_{TOTAL} \cong \frac{2400^2}{220^2} 0.05mm = 5.95mm$$

Thus, a spurious deflection of about *2.4mm per meter of board* could be expected with the described sensor configuration. An adequate amount of small-model regularization effectively mitigates this discrepancy.

Encoder

The encoder attached to the conveying system is in charge of the important task of keeping track of the board's longitudinal position during the data acquisition process.

A robust assembly is required in sawmill implementation due to the vibration levels and sawdust accumulation. The recommended mounting place is directly on the shaft moving the chain sprocket, but a decision on the details must be taken on a case basis.

For the laboratory assembly described in this work the choice was a BEI L25 rotary incremental encoder with 2500 cycles per turn, dual channel. Index was not necessary.

Appendix IV. Progressive solution

Considering equations (8):

$$\begin{aligned} a_i &= u_i + w_i \\ b_i &= u_{i+p} + w_i \\ c_i &= u_{i+p+q} + w_i \end{aligned}$$

It is attractive to think about eliminating the rigid body motion by doing

$$2\,c_i - a_i - b_i = 2\,u_{i+p+q} - u_i - u_{i+p}$$

And, in this way, write the recursion

$$u_{i+p+q} = \frac{2\,c_i - a_i - b_i + u_i + u_{i+p}}{2}$$

And solve iteratively upon having made a reasonable assumption on the first $p + q$ values.

Some numerical experimentation was made in an attempt to solve the SE in this way, but the results were found to be extremely slowly convergent or even divergent.